NASA TECHNICAL NOTE

NASA TN D-1986

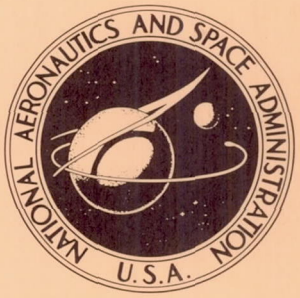

MICROMETEOROID SATELLITE (EXPLORER XIII) STAINLESS-STEEL PENETRATION RATE EXPERIMENT

by Staff of the Lewis Research Center

Lewis Research Center

Cleveland, Ohio

NATIONAL AERONAUTICS AND SPACE ADMINISTRATION • WASHINGTON, D.C. • OCTOBER 1963

TECHNICAL NOTE D-1986

MICROMETEOROID SATELLITE (EXPLORER XIII) STAINLESS-STEEL PENETRATION RATE EXPERIMENT

By Staff of the Lewis Research Center

Lewis Research Center
Cleveland, Ohio

NATIONAL AERONAUTICS AND SPACE ADMINISTRATION

MICROMETEOROID SATELLITE (EXPLORER XIII) STAINLESS-STEEL PENETRATION RATE EXPERIMENT

By Staff of the Lewis Research Center

SUMMARY

An experiment to assess the meteoroid hazard to thin stainless-steel skin material was flown as part of the Explorer XIII satellite. A total area of 3.75 square feet consisting of 3- and 6-mil-thick AISI 304 stainless-steel segments was exposed in space for a period of approximately 3 days. There were no penetrations in the exposed area during the data gathering lifetime of the experiment. This report describes the development of the experiment and the conclusions drawn from the satellite's brief lifetime in orbit.

INTRODUCTION

One primary concern for space vehicles is the meteoroid hazard. Meteoroid particles present a serious space hazard because, although they are infrequent, they have tremendous penetrating power at their very high velocities. The concern in regard to the hazard stems from studies of the protection required to reduce the probability of mission failure to acceptable values. These studies show that the hazard is, in general, common to all space systems and takes on added importance as the areas and times of exposure become greater.

The desire for experiments to measure the hazard directly resulted because early estimates of the hazard were based on a synthesis of related, but not directly applicable, data. The early estimates of the magnitude of the hazard were based primarily on (1) meteoroid velocity data obtained from radar and telescopic surveys of the larger particles entering the earth's atmosphere, (2) particle density estimates, which give values that vary by more than an order of magnitude depending on the assumptions, (3) particle flux rates obtained for very small particles by satellites (primarily microphone data) or extrapolations of ground-based radar surveys of large particles, and so forth, and (4) laboratory hypervelocity impact studies, which, in general, are not in the meteoroid velocity range. The uncertainties in the aforementioned data were compounded when combined to estimate the magnitude of the meteoroid hazard. The combined uncertainties gave penetration rate estimates that varied by as much as a factor of 1000 or more. The only logical means to eliminate this uncertainty was to measure the hazard directly.

Various methods can and will be used to obtain the desired information; however, satellites are most attractive for the initial efforts primarily be-

cause a large area-time product of exposure in space can be obtained. A large exposed area to record penetrations and a long exposure time are required to obtain statistically significant amounts of data.

Explorer XIII was the first step in the program to evaluate the hazard directly. It should be noted in this regard that the Explorer XIII experiment was severely limited in the amount of surface area that could be exposed as well as in the number of telemetry channels available. Consequently, the experiments aboard Explorer XIII (and, in particular, the one described in this report) represent a considerable compromise compared with the experiments ultimately desired. Unfortunately, a complete discussion of the general problem of evaluating the meteoroid hazard directly is beyond the scope of this report; however, the general philosophy of experiments to evaluate the hazard directly has been presented in references 1 and 2. In light of the experimental restrictions imposed by Explorer XIII, the points of view adopted in the development of the experiment described in this section were (1) to attempt to obtain at least some crude estimate of the hazard for a structural material of general interest, and (2) to develop techniques to be used in the future on either larger, more sophisticated experiments or in a "hitchhiking" capacity on other payloads.

DESCRIPTION OF EXPERIMENT

The purpose of the experiment was to detect meteoroid penetration of a surface of known material and thickness. The stainless-steel (AISI 304) material exposed was selected because of the general interest in austenitic stainless steel for space vehicles. The respective areas and thicknesses of material exposed were as follows:

(1) 3 square feet of 3-mil stainless steel

(2) 0.75 square foot of 6-mil stainless steel

These surfaces were expected to be oriented randomly in space, because the satellite was expected to tumble during most of its operating lifetime.

The element used to detect penetration of the stainless steel was a very fine gold grid that had electrical continuity. The dimensions and details of this grid are shown in figure 1. The fine gold grid was bonded to a dielectric (Mylar) material, which, in turn, was bonded to the rear (or unexposed) surface of the stainless steel. A photograph of the sensor mounted on stainless steel with lead wires attached is shown in figure 2. Penetration of the metal surface covering this grid ruptures the grid and destroys its electrical continuity. This change in continuity results in a resistance change in the telemetry circuit that modifies the frequency of one of the transmitted tone bursts. The development and usefulness of this sensor are discussed in detail in appendix A.

The 3- and 6-mil surfaces exposed were segmented into smaller areas, and these areas were monitored for penetration by means of the aforementioned sensor. The experimental approach followed in this particular experiment consisted in employing a censored life test in which, if a segment of the exposed surface received a puncture, the sensor associated with that segment would be-

come inoperative. This type of experiment has a self-storing feature and requires power only during interrogation. This feature was considered desirable for this early experiment where it might not always be possible to interrogate the system as often as wished and where data could be lost because of poor reception once the satellite interrogation was initiated. Within the design restrictions imposed, it was possible to segment the 3-mil surface into 32 segments and the 6-mil surface into 12 segments. (The segment areas used were either 9 or 18 sq in.) The restrictions imposed on the experiment in this and other respects are detailed in appendix B.

The manner in which the individual segments were grouped by telemetry channel is shown in table I. The segments were mounted on a cylindrical support structure (see fig. 3(a)); the physical order of mounting is shown in figure 3(b) in a developed view. In addition to the segments with their associated sensors, four thermistors for surface temperature measurements were located as indicated in figure 3(b).

EXPERIMENTAL RESULTS

The data from the gold grid sensor experiment are summarized in table II. Before the implications of these data are discussed, certain facets of the experimental results, which are important to their interpretation, should be noted:

(1) Explorer XIII did not achieve design orbit. Its lifetime was a little over 2 days, whereas its intended lifetime was upwards of 6 months.

(2) The large departure from the design orbit made it difficult to find the satellite and fix onto it for interrogation purposes. This resulted in usable data being obtained for only those orbits, or pass numbers, shown in table II. It should be noted, in particular, that all channels were not successfully interrogated until the ninth orbit, (pass number 9), approximately 15.6 hours after launch.

(3) Only one sensor lost continuity (an indication of a penetration) during the time the satellite transmitted data. The sensor that lost continuity was associated with one of the 3-mil-thick segments, as indicated by the fact that only seven sensors in channel 1 indicated continuity (see table II). It has been determined from data not shown in table II that the loss of continuity occurred during the launch phase and, therefore, should be ignored when the data are being analyzed.

The data shown in table II cannot be used to estimate a rate of penetration for the 3- and 6-mil stainless-steel materials exposed; however, the phenomenon of a surface in space being penetrated by a meteoroid can be though of as a statistical phenomenon. If the penetrations are considered to be a statistical phenomenon, the data in table II can be used to estimate a reasonable upper limit for the rates of penetration when the random pattern of events is known. Unfortunately, the random behavior of meteoroid events has not been well established for all classes of particles. The common assumption is that Poisson statistics describe the meteoroid population, referred to as the sporadic background, because this assumption seems physically reasonable. The data reported

in reference 3 support the aforementioned assumption; however, the data reported in reference 4 do not support it. The data of reference 4 indicated that the random deviation in the rate at which events were observed was much greater than that of a Poisson distribution. The interpretation proposed for the data of reference 4 was that a truly sporadic background does not exist, but rather that a background made up of numerous sporadic showers is indicated. It is apparent from the results of the investigations reported in references 3 and 4 that the statistical phenomena that describe the meteoroid population have not been established with any degree of certainty.

For purposes of analyzing the data from the experiment reported herein, it has been assumed that Poisson statistics are applicable. This assumption was made primarily because the Poisson relations are easily handled and because the available data do not definitely refute this physically reasonable assumption.

The rates of penetration corresponding to various assigned values of survival probability for the 3- and 6-mil surfaces were calculated by means of the following Poisson relation:

$$P_o = e^{-rat}$$

where

P_o survival probability (assigned)

r mean or average penetration rate (calculated)

a exposed area, sq ft (see table I)

t time of exposure, hr (see table II)

The calculated points are shown in figure 4 for surfaces 1 and 2. The rates corresponding to assigned survival probabilities are indicated by the symbols.

Shown also in figure 4 are the rates for assigned survival probabilities for a material thickness (surface 3) of 9.8 mils. This thickness corresponds to that used in an experiment conducted by the Goddard Space Flight Center with Vanguard III. (These results are presented here because they closely complement the results of the Explorer XIII experiment.) The material, area, and time of exposure for this experiment are given in table III along with the exposure results. (This information was previously presented in ref. 2.) It should be noted that the material exposed by Vanguard III was 27-mil-thick magnesium. In order to compare the data of table III with that of table II it was necessary to convert the magnesium thickness to an equivalent stainless-steel thickness (9.8 mils) on the basis of assumption (4) in the following paragraph.

Three estimated rate curves (also shown in fig. 4) were constructed from the following assumptions:

(1) Flux rates

Curve I - Whipple's mass-flux relation (ref. 5)

Curve II - McCracken, et al., mass-flux relation (ref. 6)

Curve III - Watson's mass-flux relation (ref. 7)

(2) Impact velocity, 15 kilometers per second

(3) Micrometeoroid density, 2.7 grams per cubic centimeter

(4) Summer's penetration criteria (ref. 8) for quasi-infinite targets multiplied by 1.5, where 1.5 is a thin-sheet correction based on the results reported in reference 9

The rate estimates shown in figure 4 as curves I to III, represent flux rates into the earth's atmosphere. In calculating the rates associated with the probabilities, no area exposure corrections were made to the area values shown in tables II and III for surface configuration, orientation in space, earth shielding effects, and so forth. The probability rates are therefore lower by a factor ranging from at least 2 to 4 than the estimated rates of curves I to III; however, applying a correction to the satellite data would not alter the conclusions to be drawn from the data. For this reason and because no simple logical correction procedure was available, the total area of the respective thickness exposed was used in calculating the probability rates.

In interpreting figure 4, it is necessary to remember that none of the surfaces exposed experienced a penetration. Therefore, it is logical to assume a reasonably high survival probability for the surfaces both individually and collectively. The survival probability to be selected as reasonable is, of course, a matter of personal choice. Within the preceding context then, figure 4 indicates that the rate estimates given by curve I are pessimistic because they produce very low survival probabilities for the exposed surfaces. In particular, if the combined survival probabilities are considered (i.e., the product of survival probabilities of surfaces 1 to 3), curve II also results, in general, in low survival probabilities. In particular, curve II appears to give rate estimates that are too high for the thinner surfaces. Curve III seems to be the most rational estimate of the rates based on the exposure data available. As a point of interest, the combined survival probability of the three surface thicknesses investigated would be 2×10^{-4}, 4×10^{-6}, and 0.97, if the penetration rates were those indicated by curves I to III, respectively.

The data obtained by the experiment are of limited value primarily because no penetrations were recorded. The usefulness of the data lies in establishing upper limits to the rates expected, but the data cannot be used to determine the actual rates prevailing or to set a lower limit. The kinds of data required to establish rates and their variations have been discussed in detail in reference 1.

There are some aspects of the information shown in figure 4 that require comment. The mass-flux relation used in constructing curve II was based on satellite microphone data. This detection system is thought to be momentum sensitive, based on calibration data for low-velocity impacts. (The pulse strength or response was found to be a linear function of impact momentum, and these results were assumed to hold for impacts at micrometeoroid velocities.)

The pulse level measured by the microphone in space is converted to a mass measurement for the impacting particles by assuming an average velocity of impact (usually 30 km/sec). Although the microphones do not measure mass directly, the data from the microphone experiment do represent essentially the only direct measurements of flux rates for the size particles that are most likely to penetrate the material thicknesses exposed by Explorer XIII. The flux rates associated with curves I and III are based on extrapolations from meteor-survey results, which involve larger mass particles. Assumptions are also necessary to convert these observations into estimates of flux as a function of mass. A full discussion of these considerations is, however, beyond the scope of this report, but they are discussed more fully in references 1 and 2.

It was noted in the discussion of figure 4 that curve III may be a reasonable estimate of the rates to expect. If the flux rates reported for the microphone data are correct, rates as low as curve III would not be anticipated unless the damage caused by micrometeoroids is much less than estimated. A temptation exists in the aforementioned regard to assume that the particles may be of very low density as postulated by Whipple, Beard, and Opik; however, it would be rather rash to infer that the particles have very low density based on the meager amount of data presently available. Such an inference would introduce difficulties in physically explaining how low-density particles of such small dimensions could exist in the solar system (see, e.g., ref. 10). It would also be necessary in this regard to demonstrate that low-density particles lack the penetrating power of denser particles of equal mass. It might be conjectured that the short exposure time of Explorer XIII surfaces occurred during a period of unusually low meteoroid activity; however, since Vanguard III data covered a period of 72 days, the short exposure time thus could not be explained on this basis. Another possibility that seems plausible is that previous satellite data may undergo some adjustment once the microphone devices receive more complete calibration. Complete calibration of these devices has not been possible in the past, because velocities in the meteoroid range were not obtainable in the laboratory and there have been other problems associated with these devices, such as thermal creaking. Other explanations or speculations could be put forward to explain the results observed. For example, the assumed impact velocity may be too great, or damage criteria developed for particles three orders of magnitude greater than those expected to be encountered are not valid when applied in estimating rates of penetration. It is quite apparent, however, that there is a need for experimental data with more statistical significance, so that it will not be necessary to resort to conjecture. A word of caution in one other respect should be expressed in regard to the Explorer XIII data. The average perigee of Explorer XIII over its useful life was less than 113 kilometers, an altitude at which meteoroid particles begin to interact rather drastically with the earth's atmosphere (i.e., meteor sightings normally occur in an altitude range of from 80 to 110 km). The data may not be representative, therefore, of results at greater perigee. Some of the ephemeris data for the satellite were as follows:

	Initial orbit based on minitrack data	Predicted
Apogee, km	1147	980.1
Perigee, km	112.8	452.6
Period, min	97.25	99.06
Eccentricity	0.07379	0.03713
Inclination, deg	37.68	37.68
Argument of perigee, deg	180.9	108.4

The skin temperatures recorded for the Explorer XIII package while in orbit are shown in table II and figure 5. Unfortunately, the data are too sketchy to trace a true temperature-time history for the package. In addition, it is difficult to give a physical explanation for the differences between the individual thermistor readings, since the satellite reportedly had not started to tumble in orbit. It is questionable, therefore, that the differences indicated are real. It is more likely that the differences noted are due to imperfect matching of thermistor characteristics (see appendix B) and telemetry system effects. The high initial temperatures are undoubtedly due to aerodynamic and rocket heating during ascent to orbit. The increasing temperatures toward the end of the satellite life are probably due to atmospheric drag heating at perigee caused by the rapidly decaying orbit. The temperatures achieved were satisfactory operating temperatures with exception perhaps of the temperatures immediately after injection into orbit.

The maximum temperature experienced during launch was estimated to be 115° F. This was well below the 150° F maximum temperature limit specified (see appendix C). The thermal control measure for the package, therefore, appear to have been adequate for both launch and orbit phases of flight.

CONCLUSIONS

The data obtained from the stainless-steel penetration rate experiment flown on Explorer XIII are limited; however, when combined with penetration data from Vanguard III, some conclusions can be drawn. Whipple's mass-flux distribution and McCracken, et al. mass-flux distribution along with the following assumptions: (1) meteoroid density, 2.7 grams per cubic centimeter, (2) meteoroid velocity, 15 kilometers per second and (3) Summers' penetration criteria yield predicted rates of penetration that are probably too high. Predicted penetration rates based on Watson's mass-flux distribution and the preceding assumptions appear to be more reasonable than the others.

Lewis Research Center
National Aeronautics and Space Administration
Cleveland, Ohio, June 14, 1963

APPENDIX A

SENSORS

Sensor Design Philosophy

The basic purpose of the desired sensor is to detect meteoroid penetration of a surface of known material and thickness. In general, there are a limited number of physical principles that can be employed to measure a penetration. The principle employed in this experiment has been described previously in the section DESCRIPTION OF EXPERIMENT.

Some of the reasons the gold grid sensor was developed are as follows:

(1) Light weight

(2) Ability to be used to sense penetrations through almost any type of material

(3) Adaptability to almost any configuration

(4) Adaptability to a wide variety of telemetry and data-handling systems

(5) Low power consumption

(6) Self-storing feature

(7) Simplicity and reliability

(8) Adaptability to future vehicles with expandable surfaces

In addition to these features, the following considerations were important in selecting a sensor:

(1) It should be able to detect the smallest hole caused by complete penetration of the test specimen.

(2) It should not have an appreciable effect on penetration of the test specimen.

(3) It should not record meteoroid impacts that do not result in penetration of the test specimen.

(4) It must be rugged enough to withstand launch conditions and the space environment.

Sensor Development

The sensor used is shown in figures 1 and 2. It is an equilateral triangle with sides 4.57 inches long and an effective area of 9 square inches. Grid

dimensions selected were 0.002-inch-wide lines and 0.002-inch-wide spaces. If an impact is centered on a space, the minimum hole size that would ensure rupturing one grid line is 0.006 inch in diameter. The minimum size hole resulting from complete penetration of 0.003-inch-thick material was estimated to be of this order; therefore, these grid dimensions were considered satisfactory. Furthermore, the area of the sensor damaged by penetration is expected to exceed the size of the hole in the test specimen. Finer grids could have been used, but development time and cost of sensors would have been greater.

Gold was selected for the grid material because of its ductility, corrosion resistance, and low resistivity. The grid thickness was only 90 microinches, so that it would have negligible effect on penetration of the test specimen. Corrosion resistance was considered essential for these thin films. Furthermore, gold is readily adaptable to the manufacturing process.

Selection of the insulating material to be used between the gold grids and the test specimen was governed by the following factors: availability in ultrathin films, resistance to space environment including vacuum and radiation, and usability over a wide temperature range. Thin films of Mylar satisfied these requirements. Selection of Mylar required selection of an adhesive that would satisfy the same requirements that were imposed on the Mylar. A thermal-setting polyester adhesive was found to be satisfactory. Mylar, 1/4 mil thick and precoated on both sides with adhesive, was used for the insulating material.

A brief description of the manufacturing process follows. The process starts with a thin sheet of copper that has a flash coating of nickel, which, in turn, is coated with a photosensitive material. The grid pattern is formed on the photosensitive material by use of a master pattern. After the unexposed material is washed off, gold is electrolytically deposited on the clean nickel surface. The remaining photosensitive material is then etched away, which leaves the gold grid on the copper and nickel substrate. The gold grid and stainless-steel test specimen are then laminated with the intermediate layer of adhesive-coated Mylar by feeding the composite structure through heated rolls. Finally, the copper and nickel are removed by etching, which leaves the exposed gold grid bonded to Mylar, which, in turn, is bonded to the stainless steel.

Each sensor was microscopically inspected for flaws or defects that might impair its function. Some bridging or shorting between adjacent lines of the grid was unavoidable, and it was necessary to determine the number of lines so bridged. The number of bridges or shorts of this type was limited to 10 percent of the total number of lines; however, the average number of shorts was less than 5 percent of the total number of lines. Electrical resistance of the sensors was 22.5 kilohms ±10 percent. After inspection, a small piece of 1/2-mil-thick gold foil was cemented to each end of the gold grid with conducting silver cement. These gold pads or terminals distributed the loading imposed on the fine gold foil by electrical connections. Silver-coated wires, 5 mils in diameter, were bonded to the gold terminals with the same conducting cement. These wires serve as an intermediate connection between the sensor terminals and the heavier gage wiring leading to the telemetry (see figs. 2 and 3).

Sensor Mounting

Sensor mounting details are shown in figures 3 and 6. The basic structure of the experiment is a cylinder of 1/16-inch-thick aluminum. Large areas, approximately 60 percent of the internal surface area, are chemically milled to a thickness of 0.020 inch for weight reduction. The remaining area forms strengthening ribs and also protects the internal wiring from meteoroid impacts. Bonded to the exterior of the cylinder is a 1/32-inch-thick sheet of silicone rubber that serves as a soft flexible backing for the sensors. The sensors are bonded to the silicone rubber, which permits some movement due to thermal expansion or contraction.

Small tubes inserted in nylon bushings through the aluminum skin serve as intermediate electrical terminals (see fig. 6). The internal wiring is soldered to these tubes on the inside of the drum. Lead wires from the sensors are inserted through the tubes and then soldered to the tubes, and the internal wiring thus forms a positive but flexible connection. A somewhat simpler mechanical connection was tried, but relative movement of the sensor and aluminum cylinder caused electrical connections to fail in some cases. Finally, the three corners of the sensors are clamped down with spring-loaded nylon washers. These washers serve as a redundant holding device for the sensors in the event that the bond between the sensor and silicone rubber should fail.

Four thermistors are located on the circumference of the cylinder approximately 90° apart (see fig. 3(b)). They are embedded in the adhesive between the silicone rubber and the sensors so as to be in almost direct contact with the sensors.

Sensor Evaluation

The effect of impact and penetration on sensors was evaluated by impacting with 10- to 20-mil-diameter glass or steel spheres at velocities to about 7500 feet per second. The particles were fired from a 220 Swift rifle. Various configurations of sensors were tested, and the previously described design was established in this manner. Some of the interesting features of this program are described hereinafter.

While the gold foil grids were still in development stages, particles were impacted on sensors made with foil strain gages to determine the effect on laminates of this type. When broken, the foil folded back on itself and thus created the possibility of a short circuit that would conceal the break by remaking the circuit. Several backing materials were tried to prevent this occurrence. Hard materials reduced the depth of penetration in the test specimen, while light, porous materials did not provide sufficient backing. A thin sheet of silicone rubber proved to be satisfactory, since it offered little resistance to the particle emerging from the test specimen but provided sufficient backing in the area immediately surrounding the penetration. The rubber backing also helped prevent rupture of the sensor due to an impact that did not completely penetrate the test specimen. When the gold grids became available for testing, it was discovered that peeling or folding was not a problem with these sensors. Unfortunately, sufficient time was not available to find a lighter substitute

for the 1/32-inch-thick silicone rubber that had already been incorporated in the design. The silicone rubber used, therefore, represented a slight weight penalty.

Several dielectric materials besides Mylar were tried. One of the more promising materials was a vapor-deposited film of silicone monoxide; however, the silicone monoxide film crazed and thinned down during partial or complete penetration of the stainless steel and thus created a possibility of shorts between the gold grid and the test specimen. Consequently, it was not considered suitable as a dielectric material.

Smaller glass particles, approximately 5 mils in diameter, were also used to obtain partial penetrations of the test specimen. Despite the violent cratering action and bulging of the test specimen in the vicinity of the crater, the gold foil did not rupture. Thus, it was concluded that the sensor would detect only those impacts resulting in complete penetration of the test specimen. Attempts to penetrate the stainless steel and at the same time to make holes sufficiently small so as not to rupture the grid were not successful because of equipment limitations. The smallest holes generated by impacting particles were 6 mils in diameter, and these were more than sufficient to rupture the grid. Continuity of the sensor was disrupted in all cases of complete penetration. The sensors were also checked for short circuits in the vicinity of the penetration that might possibly remake the circuit. This condition did not occur in any of the 50 or more penetration tests. Although the impacts and penetrations in these tests may not be truly representative of meteoroid impacts, they are believed to give a fair indication of the behavior of the sensors.

APPENDIX B

DESIGN CONSIDERATIONS

Design Restrictions

There were certain design restrictions placed on the experimental package that influenced the design of the experiment greatly. These restrictions or requirements are discussed in the following paragraphs.

Telemetry. - To obtain redundancy in the satellite telemetry system, two independent 48-channel systems were used. This particular experiment was allotted three frequency channels and two time channels in each system. The frequency channels were used to interrogate penetration sensors, and the time channels were used to measure skin temperature. The details of the circuitry employed are described subsequently.

Weight and area. - The total weight of the experiment including any support structure, wiring, and so forth, was restricted to 5 pounds. The area available for exposing skin samples was approximately 4 square feet.

Configuration. - The area allotted the experiment was a cylindrical area located around the nozzle of the fourth-stage rocket.

Thermal control. - The experiment had to function in the space environment with only passive means available for controlling temperature. Heating due to fourth-stage rocket combustion and aerodynamic friction on ascent was also controlled by passive means; however, an aerodynamic heat shield was provided that was jettisoned after third-stage burnout.

Reliability. - The experiment was required to survive launch conditions and to be able to operate in the space environment for a period of at least 6 months.

Circuit Design

The design of circuits connecting the grid sensors to the telemetry system was a problem of matching the characteristics of the sensors to those of the telemetry system. The electrical characteristics of the sensors are those characteristics of a resistor with a nominal room-temperature resistance of 22.5 kilohms. This resistance has a positive temperature coefficient corresponding to that for gold of about 0.0034 ohm per ohm per ^{o}C. When a sensor is penetrated by a particle that disrupts the grid, the resistance goes nominally to infinity.

The frequency channels take a 0- to 2.5-volt full-scale signal across a 10-kilohm resistor. The time duration channels measure a resistance with a full-scale value of 5 kilohms. Both the frequency and time channels are best utilized for making analog measurements; however, the disruption of the grids, which were interrogated by means of frequency channels, is a digital measure-

ment. To utilize the frequency channels, therefore, it was necessary to obtain a discrete change of frequency each time a grid was disrupted. The minimum change in frequency that could be detected was estimated to be 10 percent of full scale. This minimum resolution was based on the estimated signal to noise ratio expected for the telemetry system and receiving equipment employed and for the intended orbit.

A frequency channel circuit that achieves a minimum full-scale change of 10 percent each time a grid is disrupted is shown in figure 7. Eight sensors represented by resistors R_S each with a series resistor R_L, are connected in parallel between the power supply and a 10-kilohm input resistor R_I. The series resistor R_L is large compared with the sensor resistor R_S and input resistor R_I such that each of the eight legs approximates a constant current source to R_I. The voltage across R_I is then a direct measure of the number of intact sensors in that channel. To maintain a minimum change in input signal of at least 10 percent of full scale when one sensor opens, the maximum number of legs is limited to eight.

As a result of satellite development changes, the grid sensor developed was not tailored to the specific telemetry channel assignment that evolved. The area assigned to the experiment was initially portioned into 60 segments of approximately 9 square inches and grid sensors 9 square inches in area were developed. An arrangement of sensors by channels that utilized the full area allotted and satisfied the aforementioned circuit restrictions is shown in table I and figure 3(b). Three channels used the circuit described previously. Sensors on two channels were doubled; that is, two sensors were tied in series to form the resistor R_S. One channel employed only four legs in parallel with one sensor in each leg. The minimum voltage change per break across resistor R_I is shown in table I for each circuit arrangement.

It should be noted that preflight calibrations of the frequency channels indicated a slightly lower sensitivity than that expected. The minimum change due to a sensor penetration is approximately 9 percent rather than 10 percent. This slight reduction in sensitivity is due to nonlinearity of the voltage to frequency converter of the telemeter.

The temperature sensitivity of the circuit employed is low because of the relative values of R_L and R_S. The most temperature-sensitive circuits, of course, are those circuits (i.e., channels) employing two sensors per leg. As an indication of the effect of temperature on the signal output, the percentage of signal change resulting from a 100° C change in temperature of all the sensors in a channel is also given in table I. If large temperature variations are actually encountered during the life of the satellite, the data will be temperature corrected by use of the skin temperature measurements described in the following paragraph.

The remaining four time-duration channels of telemetry were used to measure the temperature at four points on the surface of the experiment. These measurements were made with subminiature head-type thermistors. The four thermistors used were matched to within ±2° C, so that a single calibration curve would suffice. These thermistors were shunted with a 5-kilohm resistor to

limit the maximum resistance measured by these time-duration channels.

Selection of Skin Thickness and Area Distribution

The area and thickness distribution employed in the experiment is shown in table I and figure 3(b). Within the restrictions already outlined, the skin thickness and area distribution were selected based on the following:

(1) The experiment would have a nominal lifetime of 6 months, although it was hoped a longer lifetime would be achieved.

(2) The average rates of penetration expected were estimated as in reference 1. Based on these average penetration rates and within the area restrictions imposed, thicknesses were selected that would yield data within 6 months. The desire to expose the maximum practical thickness was also used as a criterion in selecting material thickness (i.e., maximum thickness consistent with the requirement that any results have statistical significance).

(3) It was recognized that the rates predicted were at best only crude estimates and that the random fluctuations about these average rates might be quite large. Rates at least two orders of magnitude greater or less than those predicted could be recognized with the skin thickness and area distribution selected. If the rates were two orders of magnitude greater than those expected, portions of the 6-mil surface should survive long enough so that it would be recognized that breaks (disruption of the electrical continuity in individual legs of the parallel circuits described previously) were occurring as the result of penetrations of the surface material and not as a result of some experiment malfunction. If the rates were two orders of magnitude less than those predicted, there should be a sufficient amount of 3-mil surface area exposed that some penetrations would be recorded in a 6-month period and, as a result, would show that the experiment was performing satisfactorily.

(4) The satellite was expected to tumble in space, and, therefore, the arrangement of the sensors on the periphery was not considered of consequence. To correct for temperature effects, however, it was desirable to have all sensors in a given telemetry channel at approximately the same temperature and to have a measurement of this temperature. All sensors in a given channel were grouped together, therefore, in the vicinity of a thermistor. The exception was channel 6 for which it had been planned to expose bare sensors without protective stainless-steel covers; however, a lack of time and other more pressing problems did not permit this development.

(5) The considerations in item (4) were also influenced by the fact that breakage of individual legs in a channel could not be distinguished from one another as a result of the circuit employed (i.e., only the number of legs lost per channel as a result of penetrations could be determined).

(6) Both material thicknesses (3 and 6 mil) were used on telemetry channels A and B. Thus, in the event of a failure of either telemetry system, the experiment would simply be reduced in scale.

(7) It was desirable to divide the 3- and 6- mil surfaces into as many segments as possible for statistical reasons (see ref. 1).

Thermal Control

The construction of the experimental package utilized Mylar and adhesives, which were essentially in intimate contact with the stainless-steel surface being exposed. The adhesives, in particular, made it desirable to limit the surface temperatures to a maximum of approximately 200° F. For this reason, the temperatures that would result from exposing bare stainless steel could not be tolerated because stainless steel has a ratio of solar absorptivity to low-temperature emissivity α/ϵ of about 8. It was necessary, therefore, to lower the exposed surface α/ϵ ratio preferably to some value less than 1.0.

The temperatures of a number of satellites have been successfully controlled in the previous manner; however, the coatings employed have, in general, been quite thick. In addition, only the internal temperatures of the satellite (in particular the telemetry package) were of concern, and considerable fluctuation of outer skin temperature was tolerated. The thermal requirements of this experiment necessitated that the exposed skin itself must not exceed a given temperature, and any coatings used to reduce the maximum temperature must be thin enough so that the penetration phenomena are not seriously compromised. Information of this character was not available; and, therefore, it was necessary to develop the data. The data on thin coatings were obtained with the space-simulator equipment described in appendix D. A number of the coatings investigated were of the organic type (white paint), which is affected in particular by the ultraviolet portion of the solar spectrum. The effect of ultraviolet radiation on the coatings was investigated by using the equipment described in appendix E. Additional elimination of coating materials was done in the course of the thermal-vacuum test conducted on sensor assemblies described subsequently by exposing specimens mounted in the vacuum chamber to ultraviolet radiation entering the vacuum chamber through a quartz window and emanating from an ultraviolet lamp.

The ratio of α/ϵ required to control the experiment temperature could not be determined precisely because the experiment had to be designed without a full knowledge of the temperature control to be applied to adjacent structures. In addition, the heat-conduction characteristics between the experiment and the adjacent structure were not known. It was anticipated, however, that the adjacent structures or experiment would run hotter. A very difficult thermal gradient problem also occurred with the ring assembly used. The ring was so thin that no appreciable conductions of heat around the ring could be relied on to even out the temperatures. Thus, any sensor facing the sun could, to a large extent, only reject heat by radiating it back to space if conduction from adjacent structures is ignored. In the event the adhesive bonds did not hold (and the structure was held only by the mechanical connections discussed previously), the condition of no conduction just discussed would be very close to the actual situation prevailing. The maximum temperature of a sensor in this detached state would be almost entirely a function of the α/ϵ ratio of the surface. For this reason, the α/ϵ ratio had to be 1.0 or less because the maximum temperature that could be tolerated was about 200° F. It was decided in the light of

the problems just discussed to limit the maximum temperature and accept any resulting thermal gradients with the hope that the gradients would be alleviated by conduction from adjacent structures.

The coating or surface treatment that appeared most satisfactory for the application in mind was obtained by treating the stainless steel by a commercial process. The stainless steel is subjected to a hot salt bath that forms a mixed iron oxide surface layer, which is negligibly thin (perhaps no more than a few microns) and has a flat black appearance. The α/ϵ ratio measured in the space simulator for this coating had a nominal value of approximately 0.97. This value of α/ϵ would be satisfactory if the experiment were isolated from the remainder of the experiments, which were designed to run hotter. Some conduction of heat from adjacent experiments were expected, and, thus, a lower value of α/ϵ should be obtained. For this reason and because low skin temperatures were no apparent problem, it was decided to apply a coat of white paint over the black stainless-steel surface to drop the α/ϵ ratio still further. The paint selected for this purpose from a number that were investigated had a titanium dioxide pigment. A spray method of application was used to obtain a very thin, uniform coat. The spray coating lowered the α/ϵ ratio of the surface to a value of approximately 0.65. (Dipped coatings gave lower α/ϵ ratios, but there did not appear to be any practical method of applying the coatings to the final assembly in this manner. In addition, it was much more difficult to control the coating thickness when a dip process was used.) Since there was some concern that the properties of this coating would be seriously altered by the solar ultraviolet radiation, the specimens were exposed under vacuum conditions to the equivalent of 1200 hours of solar ultraviolet radiation (approx. equivalent to 6 months of exposure on the satellite), and the ratio of α/ϵ measurements was taken again. Although the coatings had turned brown on exposure to the ultraviolet radiation, the α/ϵ ratio had only increased to approximately 0.77. The thermal control coating used for the experiment then consisted of blackening the stainless steel and then spraying white paint over the black surface to a nominal thickness of 0.5 mil. (As a point of interest, the emissivity value measured for the surface was 0.95 at a specimen temperature of 80° C.)

Although other coatings were investigated, only the thermal control coatings finally selected have been described herein. It might be noted, however, that paints have many advantages as thermal control coatings. Chief among these advantages is ease of application, even as a final step in the process of fabrication.

Heating of the experiment during the launch phase due to aerodynamic friction and heat transmission through the rocket casing and nozzle was also of concern; however, this aspect of the thermal design was handled by those persons responsible for the thermal design of the total payload. It was specified, however, that the combined aerodynamic and rocket heating should not cause the experiment temperature to exceed a maximum of 150° F.

APPENDIX C

ENVIRONMENT TEST

The prototype and flight assemblies of the Lewis meteoroid penetration experiment were exposed to environmental tests including vibration, acceleration, shock, and thermal vacuum. The prototype was tested to values 50 percent greater than those anticipated during launch, while the flight assemblies were tested to anticipated values. For all tests, the assembly was restrained in a manner to simulate as near as practical actual mounting on the fourth-stage rocket. These were additional to tests of the complete satellite assembly conducted by Langley. Tests were conducted also on individual sensor assemblies.

Equipment

Thermal vacuum. - Equipment used for the test was essentially an isothermal enclosure for the test specimen inside a vacuum chamber. The enclosure was electrically heated and cooled by liquid nitrogen. Thermal cycling tests were conducted during regular working hours only because automatic equipment was not available. About three cycles per day were possible. Vacuum, however, was maintained overnight. Temperature and electrical resistance of the sensor were continuously monitored during the test. The sensors were visually inspected when each test run was completed.

Vibration. - The required vibration tests were conducted on a 1500-pound-force shaker. A controller together with an appropriately placed accelerometer maintained a constant sinusoidal amplitude at the accelerometer location as the frequency was varied.

The instrumentation for the vibration tests consisted of a piezoelectric accelerometer and matching amplifier system, a direct-current amplifier, a detector-filter, and a recording oscillograph, as shown in figure 8. Also shown is the driving force recording method. All components except the detector-filter were commercially available items. Performance of the instrumentation was satisfactory.

Shock. - The shock test equipment consisted of a platform mounted between two vertical guide rods. Wedges were attached to the bottom of the platform to control deceleration. To produce the shock, the platform with wedges, mounted test package, and attached instrumentation were elevated to a height of 42 inches above the rest position. A solenoid-operated release allowed the assembly to fall freely to a bed of sand. The wedges entered the sand and provided the controlled deceleration force. The equipment used was commercially manufactured. Results were reproducible to about ±10 percent.

Spin. - The purpose of the spin test was to apply a sustained axial and radial acceleration to the test package. The forces were applied in three directions. The package was spun about its axis of symmetry (vehicle thrust axis), it was spun about an axis perpendicular to the thrust axis with the force along the thrust axis, and it was spun about an axis perpendicular to the thrust

axis with the force along the reverse thrust axis. The package was rotated on the horizontal platform of a commercial spin table. Table speed was adjusted manually.

Test specimen mounting. - Both flight and prototype assemblies were bolted to a test platform by means of the flange on the assembly that was used to mount the experiments on the rocket. The test platform consisted of a baseplate and a simulated section of the skirt around the nozzle of the fourth-stage rocket. all loads and vibrations were applied to or through the baseplate, which simulated the rocket. These loads were then transmitted through the mounting flange and simulated skirt and thus approximated the actual rocket loading. The individual sensors tested were also mounted to simulate the actual loading configurations.

Test Results

Thermal vacuum. - The tests conducted with individual sensor assemblies are summarized in table IV. Sensors 1 to 3 were laminations of 0.006-inch stainless steel, 1/4-mil Mylar insulation, and gold foil grid, respectively, and a 1-mil cover of Mylar. Sensor 4 was identical except that the 1-mil Mylar cover was omitted. Sensors 5 to 7 were identical to sensors 1 to 3 but were bonded to silicone rubber and aluminum.

To of the three sensors that failed (lost electrical continuity) did so at temperatures near 300° F. Sensor 1 failed when the temperature of the isothermal chamber overshot the desired temperature (230° F) and climbed to 290° F. When the temperature was intentionally raised to 300° F after 382 hours of soaking at lower temperatures, sensor 3 failed. The failure of sensor 2 was apparently due to thermal shock when room air was rapidly bled into the test chamber. In all three cases, failure amounted to disruption of the electrical continuity of the grid; however, microscopic examination of the sensors did not reveal the location of the break. All other sensors retained their continuity during and after the test. It appears, therefore, that individual sensors will withstand soaking at 250° F or cycling between -50° and 250° F for long periods.

In fabricating the prototype and flight packages, the sensors were bonded to the silicone rubber backing by soaking at temperatures in excess of 200° F for 12 hours. Thus, all sensors were exposed to this temperature at atmospheric pressure. The flight packages were exposed to a vacuum of approximately 10^{-6} millimeter of mercury for 200 hours or more. During this time, 10 or more thermal cycles ranging from -50° to 150° F were completed. In addition, one package was tested for five thermal cycles from -50° to 150° F at atmospheric pressure. For the thermal-vacuum tests, the experiment was mounted on a skirt simulating the mounting on the fourth-stage rocket. One complete cycle between -50° and 150° F required about 4 to $4\frac{1}{2}$ hours.

During all thermal and thermal-vacuum tests, a continuous check on the resistance of the sensors and thermistors as well as checks for shorts to ground was provided by a semiautomatic checking device. This device reported a fault if the resistance did not fall within prescribed limits, which were governed by the temperature variation of resistivity, or in the case of shorts to ground, if the resistance dropped below about 17 megohms.

The sensors would not tolerate as high a temperature when mounted to the aluminum cylinder as when they were mounted to a flat plate. Sensors mounted on a flat plate, as described previously, withstood temperatures in excess of 250° F. Distortion of the aluminum cylinder at elevated temperatures caused relative movement between the sensors and the cylinder, which caused a few sensors to fail (lose continuity). Therefore, the test temperature was reduced to the more realistic temperature cited previously (150° F). In this regard, it might be mentioned that other mounting schemes were available to alleviate this condition; however, because it was not critical that the experiment be designed to withstand higher temperatures and because time was short, these schemes were not incorporated in the present satellite.

A few sensors failed during the bonding operation at 200° F and initial thermal-vacuum tests. These were believed to be defective sensors, and when they were replaced, the assembly was retested with satisfactory results. No other detrimental effects of thermal or thermal-vacuum environment were observed.

Vibration. - The tests with individual sensors were conducted with sensors mounted on silicone rubber and fastened to an aluminum sheet in the same manner as it would be on the flight assembly. Sinusoidal vibrations from 500 to 2000 cycles per second and back at a sweep rate of 2.8 octaves per minute were applied to the sample. The acceleration varied between 43 and 47 g's during the test. Electrical continuity of the sensors was maintained throughout the test. Visual inspection of the sensors after test completion revealed no damage.

The flight assemblies were subjected to vibrations along the thrust axis, as listed in the following table:

Flight assembly	Exciter frequency, cps	Peak amplitude, g's	Sweep rate, octaves/min	Duration, min
1	50 to 2000	5	2	3.0
1	50 to 2000	5	4	1.5
1	500 to 2000	10	4	0.5
2	50 to 2000	5	2.8	1.65
2	500 to 2000	10	2.8	0.712

The assemblies were resonant at approximately 300 to 1000 cycles per second; as a result, the amplitude increased by a factor of 10 or more. Plots of the variations in acceleration for the second flight assembly are shown in figure 9. Accelerometer 1 was on the driving plate to which the flight assembly was attached. Accelerometers 2 and 3 were attached to the flight assembly. No adverse effects on the assemblies were noted as a result of the tests.

Shock. - Both individual sensor assemblies and complete flight assemblies were tested in both directions parallel to the thrust axis. Drop-test results for one flight assembly in one direction are shown in figure 10. A peak acceleration of approximately 77 g's with an average impulse of approximately 44 g's for 0.01 second was experienced. No adverse effects on the assemblies were noted as a result of the tests.

Spin. - The test package was bolted to the spin-table platform, which was spun about an axis to simulate radial loads developed by the spinning rocket. For the tests where rotation was about an axis perpendicular to the axis of symmetry (to simulate thrust loads), a suitable jig was constructed to permit balancing of the assembly for both the thrust and reverse-thrust spin tests.

Radial accelerations of 50 g's were applied to the sensor assemblies mounted either as individual assemblies or as part of the flight assemblies. As a result of the finite radius employed in the aforementioned jig, uniform axial accelerations in the thrust and reverse-thrust directions could not be obtained. The simulated thrust acceleration applied varied from a minimum of about 15 g's to a maximum of about 22 g's for the sensors in a flight assembly. These accelerations were applied for a period of 30 seconds. No adverse effects on the assemblies were noted as a result of the tests.

APPENDIX D

MEASUREMENT OF ABSORPTIVITY-EMISSIVITY RATIO

Thermal-Vacuum Chamber

Measurements of α/ϵ of various coatings were made in a space simulator. This facility consists of a vacuum chamber with an internal structure for mounting and instrumenting a test specimen. The interior walls of the tank were cooled to act as a radiant heat sink, and one end was fitted with a window through which the test specimen was illuminated with simulated solar radiation.

A section view of this facility is shown in figure 11. The test specimen support is shown mounted on a removable back flange. Details of the support and the specimen mounting arrangements will be discussed in more detail subsequently. The interior surface viewed by the test specimen is that of a cylindrical sleeve at liquid-nitrogen temperature. The hollow walls of the sleeve are filled with liquid nitrogen through the fill tube. Attached to the interior of the sleeve is a spiraled baffle, which prevents reflection of the incoming light from the sleeve onto the test specimen. Teed to the bottom of this tank is a flange, which connects to the vacuum pump system. The pumping system consists of an ionic-type pump (ultimate pressure, $<10^{-9}$ mm Hg; rated speed, 250 liters/sec) and a conventional roughing system. Operating pressure on this facility is less than 5×10^{-7} millimeter of mercury as measured by an ionization gage located just above the vacuum pump flange. At the front end flange of the tank, a quartz window is mounted through which the simulated solar radiation is admitted to the chamber.

Figure 12 shows the test specimen support with a specimen in place. Supported off the main flange is a copper plate, which can be heated with "sandwiched-in" heater wire. The center section of this plate has four spring-loaded posts from which the test specimen is suspended by cotton thread. Electrical connections for the heater wires and temperature sensors are made through glass to metal seals in the back flange.

Figure 13(a) shows the assembled tank and its position with respect to the solar simulator.

Test Specimen Preparation

Coatings were applied to 0.006-inch-thick stainless-steel sheets approximately 2 inches square, and 1-inch-square test specimens were selected from this sample on the basis of evenness of coating, as judged by visual inspection. A thermistor was then bonded to the center of the back surface. Thermistors were also used to measure the temperature of the copper backplate. All thermistors were bead type, of commercial manufacture.

Chamber Operation

Measurement of the α/ϵ ratio for a test specimen was accomplished in the following manner. The test specimen, prepared as described previously, was mounted in the chamber, and the measuring circuits were checked for proper operation. After the tank was evacuated, liquid nitrogen was put into the hollow wall of the sleeve in the tank, and the solar source was started. An automatic controller on the solar source maintained a constant light intensity in the plane of the test specimen. Changes in temperature of the test specimen were noted, and heaters on the backplate were manually controlled, so that the backplate and the test specimen were at the same temperature. The test specimen temperature was recorded when equilibrium conditions were achieved.

If the solar radiation incident on the test specimen has an intensity of one solar constant, the α/ϵ ratio can be calculated from the equation

$$\frac{\alpha}{\epsilon} = \frac{\sigma T_e^4}{s}$$

where

$\frac{\alpha}{\epsilon}$ ratio of solar absorptivity to total hemispherical emittance

σ Stefan-Boltzmann constant

T_e absolute equilibrium temperature of the test specimen

s solar constant at mean earth-sun distance, 140 mw/cm^2

Errors in Simulation

It is of interest to examine sources of error and the effects of these errors in such a measurement. Consideration of the equation used to calculate α/ϵ will show that, since the temperature is raised to the 4th power, small percentage errors in temperature will produce four times as much error in α/ϵ as will the same percentage error in other terms. With this in mind, sources of error can be considered under general categories: (1) temperature measurements, (2) heat losses not accounted for in the calculation, (3) imperfect space simulation, (4) viewing loss, and (5) imperfect solar simulation. The last of these has been included here only for completeness; errors in solar simulation are discussed in the section Simulated Solar Radiation.

Temperature errors arise from calibration techniques, errors in the measurement of resistance, and self-heating effects. The thermistors used in these measurements were calibrated at one point, which defines R_o and T_o in the thermistor resistance equation

$$R = R_o e^{B\left(\frac{1}{T} - \frac{1}{T_o}\right)}$$

where

R resistance at temperature T

R_o resistance at temperature T_o

B constant supplied by manufacturer

Sample measurements have indicated an error of $\pm 2^\circ$ K due to variations in B. Estimates of errors of the resistance measurment amount to $\pm 1^\circ$ K. The power dissipated in the thermistor produces an estimated 0.1° K temperature rise; self-heating effects can be completely neglected. As a result, if the probable error in temperature is taken as $\pm 3^\circ$ K, the probable error in α/ϵ is ± 4 percent.

Estimates of heat losses from the test specimen by radiation from the back side and by conduction through supports and thermistor leads would indicate a probable error of ± 1.5 percent in α/ϵ.

Imperfect space simulation includes a number of effects. The error caused by using a 77° K heat sink (higher than in space) and then disregarding this term in calculating α/ϵ is approximately 0.3 percent. This value is based on an equilibrium temperature of 350° K and would be less for higher equilibrium temperatures. Errors result from reflections of emitted radiation back to the test specimen. These include specular reflection off the window and diffuse reflection from all interior surfaces viewed by the test specimen. Estimates indicate errors in α/ϵ from these sources to be less than 0.5 percent. Errors can also result if the pressure is not maintained sufficiently low to make the thermal conductivity of the residual gas negligible. Operating pressures of 5×10^{-7} millimeter of mercury rule out such errors.

The viewing loss due to the geometry employed also introduces a small error. In space at the mean earth-sun distances, the sun occupies approximately 0.1 percent of the field of view of a surface illuminated by the sun. In the space simulator the window occupies approximately 1.0 percent (as defined by the angle β of fig. 11) of the field of view of the test specimens. Although this area is higher by a factor of 10, its effect (the amount by which the heat sink area is reduced) is less than 1.0 percent.

On the basis of these considerations and excluding the errors due to imperfect simulation of solar radiation, the probable error in α/ϵ can be taken as ± 4.3 percent.

Simulated Solar Radiation

Equipment. - The source of radiation for simulating the intensity and spectral distribution of the sun's radiation was a special carbon arc lamp. The positive electrode was a 13.6-millimeter-diameter rod of special composition. The negative electrode was 11.1 millimeters in diameter. The arc consumed 135 to 145 amperes at 55 volts.

The radiant energy from the arc was collected and transferred to the test specimen by a specially designed optical system (see fig. 13(b)). All elements of the system were fused silica. To transfer the radiant energy, an image three times normal size was formed in the plane of a projection lens by two condensing lenses. The projection lens images one of the condensing lenses into the plane of the test specimen. This arrangement ensures uniformity of radiance on the test specimen. Since only flat surfaces were tested, a collimated light beam was not necessary.

The intensity of the radiation at the specimen plane was measured with a thermopile. During system operation, a closed-loop control system monitored and regulated the radiation intensity falling on the specimen. A selenium photovoltaic sensor was used to measure the radiation for monitoring purposes. This sensor was located at the mirror image of the specimen. The radiation received by the sensor was reflected from a window surface in the optical path. Any variation in sensor output was amplified and caused the condensing lens assembly to move. Motion of the lens altered the amount of radiation intercepted by the condensing lens system in such a way as to restore the initial radiant intensity. The equipment was capable of continuous operation for up to 35 minutes.

Measured spectrum. - The spectrum of radiation from the solar simulator is shown in figure 14. The spectrum measurement was made on an infrared spectroeter with a lithium fluoride prism and a lead sulfide detector. The instrument was calibrated with a National Bureau of Standards tungsten standard lamp.

Errors. - Subsequent to the use of the solar simulator for the purposes described in this report, an improved calibration device was acquired. This standard was an Angstrom, compensated pyroheliometer. Calibration of the thermopile with the pyroheliometer indicated an error of +7 percent in the assumed total intensity. Therefore, the intensity actually used was 93 percent of a solar constant. A value of 1395 watts per square meter was used as equivalent to one solar constant. The spectrum measurements were made with the total radiation under automatic control, as described previously. The optics of the system were included in the light path. The measurements were corrected for scattered light and detector noise level. No statement on the accuracy of the measurements can be made. Reproducibility over a period of 2 months was ±5 percent.

Uniformity of radiant intensity on the specimen was measured. A magnesium oxide specimen was substituted for the experimental specimen. The brightness of the surface of the magnesium oxide specimen was measured. Five percent of the total area was used for each measurement. The brightness of the surface was uniform to within ±3 percent at any point on the specimen.

APPENDIX E

ULTRAVIOLET DEGRADATION MEASUREMENTS

Description of Equipment

The source of the ultraviolet radiation was a 900-watt high-pressure mercury arc (air cooled). The light from the source was collected and directed to the sample by a fused silica optical system. The specimen was irradiated with a strongly convergent beam.

The specimen was mounted inside a 5-inch-diameter Pyrex tee. The tee was mounted on an ion vacuum pump. The radiation from the lamp enters the tee through a 1/2-inch-thick fused silica window.

Test Specimen Preparation

The specimens to be irradiated consisted of a 1-inch-square stainless-steel sheet. The coating to be tested was applied to one side only; the specimen was then fastened tightly to a copper plate. The copper plate was supported by means of four stainless-steel posts approximately 2 inches long. Heater wires were wrapped around the supporting posts. By manual adjustment of the power supplied, the temperature of the specimen could be controlled. The temperature of the specimen was measured by a thermistor attached to the side of the copper mounting plate opposite the specimen.

Test Procedure

Before the end plate supporting the specimen was fastened to the Pyrex tee, a measurement was made of intensity of the radiation reaching the specimen location. The end plate was then attached, and the system was evacuated. A sample of the beam was monitored to ensure that constant power was being received by the specimen. Data recorded were time of irradiation, specimen temperature, pressure in the test chamber, heater power, and source intensity. The product of intensity of radiation reaching the specimen and time of exposure is the total exposure of the specimen.

Errors

Information pertinent to estimating errors in the experiment is given subsequently.

The spectrum of the lamp is given in reference 11. The spectrum shown therein is modified in this application by passing through approximately 1 inch of fused silica.

The amount of radiation striking the specimen with a wavelength of 0.25 to 0.4 micron was measured with a thermopile. The same thermopile was used in

measuring the ultraviolet portion of the carbon-arc solar-simulator radiation. The ultraviolet radiation intensity was measured by eliminating the visible and infrared radiation with Corning 9863 and 3486 filters.

The number of solar constants of ultraviolet radiation incident on the specimen was calculated from

$$N = \frac{(I_1 - I_{1+2})}{KI_0}$$

where

N number of solar constants incident on thermopile

I_1 millivolt output of thermopile with 9863 filter in place

I_{1+2} millivolt output of thermopile with 9863 and 3486 filters in place

I_0 millivolt output of thermopile in sunlight or of carbon-arc solar simulator in band of wavelength ranging from 0.25 to 3.0 microns

and K is defined as

$$K = \sum_{\lambda=0.25}^{0.4} T_\lambda J_o = 0.067$$

where

T_λ transmission of 9863 filter

J_o fraction of total solar radiation in wavelength band from Johnsons data

REFERENCES

1. Davison, Elmer H., and Winslow, Paul C., Jr.: Space Debris Hazard Evaluation. NASA TN D-1105, 1961.

2. Davison, Elmer H., and Winslow, Paul C., Jr.: Direct Evaluation of Meteoroid Hazard. Aerospace Eng., vol. 21, no. 2, Feb. 1962, pp. 24-33.

3. Weiss, A. A.: The Limitations of Narrow-Beam Radio Equipments in the Detection of Weak Meteor Showers. Jour. Atmospheric and Terrestial Phys., vol. 14, 1959, pp. 19-30.

4. Gallagher, P. B., and Eshelman, V. R.: "Sporadic Shower" Properties of Very Small Meteors. Jour. Geophys. Res., vol. 65, no. 6, June 1960, pp. 1846-1847.

5. Whipple, Fred L.: The Meteoritic Risk to Space Vehicles. Paper 499-57, Am. Rocket Soc., Inc., 1957.

6. McCracken, C. W., and Alexander, W. M.: The Distribution of Small Interplanetary Dust Particles in the Vicinity of Earth. Smithsonian Contributions to Astrophys., vol. 7, 1963, pp. 73-75.

7. Watson, F. G.: Between the Planets. Rev. ed., Harvard Univ. Press (Cambridge), 1956.

8. Summers, James L.: Investigation of High-Speed Impact - Regions of Impact and Impact at Oblique Angles. NASA TN D-94, 1959.

9. Kinard, William H., Lambert, C. H., Jr., Schryer, David R., and Casey, Francis W., Jr.: Effect of Target Thickness on Cratering and Penetration of Projectiles Impacting at Velocities to 13,000 Feet per Second. NASA MEMO 10-18-58L, 1958.

10. Alexander, W. M., McCracken, C. W., Secretan, L., and Berg, O. E.: Review of Direct Measurements of Interplanetary Dust from Satellites and Probes. X-613-62-25, NASA, 1962.

11. Anon.: Application Data and Accessory Equipment for Use with A-H6 and B-H6 Mercury Lamps. GET-1248-C, General Electric Co.

TABLE I. - EXPERIMENT PARAMETERS

Channel	Exposure parameters					Telemetry circuit parameters					
	Number of segments	Area per segment, sq in.	Thickness, in.	Material	Total area, sq ft	Number of parallel legs	Sensors in series per leg	Series resistor, R_L, kilohm	Minimum voltage change per break (percent of full scale)	Voltage change due to 100° C temperature change of all sensors in one channel (percent of full scale)	Telemetry system
1	8	18	0.003	Stainless steel	1	8	2	264	10.4	4	A
2	8	18	0.003	Stainless steel	1	8	2	264	10.4	4	A
4	8	9	0.003	Stainless steel	0.5	8	1	284	10.4	2	B
5	8	9	0.003	Stainless steel	0.5	8	1	284	10.4	2	B
6	8	9	0.006	Stainless steel	0.5	8	1	284	10.4	2	B
3	4	9	0.006	Stainless steel	0.25	4	1	132	20.8	4	A

TABLE II. - ORBITAL TELEMETRY HISTORY FOR GOLD GRID SENSOR EXPERIMENT

[Launch date, Aug. 25, 1961.]

Orbit (pass) number	Date	Starting time of recording, Greenwich mean time	Minitrack recording station	Time in orbit, hr	Number of segments surviving, by channel numbers						Thermistor temperature, °C (see fig. 3(b))			
					1	2	3	4	5	6	A	B	C	D
Launch	25	1829:44	Blossom Point	----	--	--	--	--	--	--	--	--	--	--
1	25	2009:57	Blossom Point	1.67	--	--	--	8	8	8	--	--	43	37
1	25	2011:00	Grand Forks	1.68	--	--	--	8	8	8	--	--	43	41
9	26	1002:40	Antofagasta	15.55	7	8	4	8	8	8	-5	-2	-1	10
14	26	1511:00	Blossom Point	20.68	--	--	--	8	8	8	--	--	7	3
14	26	1513:30	Fort Myers	20.71	7	8	4	8	8	8	0	3	8	3
15	26	1651:33	Blossom Point	22.37	7	8	4	8	8	8	3	9	10	7
15	26	1652:00	Fort Myers	22.38	7	8	4	8	8	8	4	7	10	5
16	26	1834:30	Fort Myers	24.08	7	8	4	8	8	8	8	13	13	10
22	27	0440:00	Santiago	34.16	7	8	4	8	8	8	9	10	11	9
23	27	0620:10	Santiago	35.83	7	8	4	8	8	8	6	6	11	8
24	27	0803:14	Antofagasta	37.55	7	8	4	8	8	8	-5	-2	3	0
29	27	1538:45	Woomera	45.15	7	8	4	8	8	8	11	6	13	11

TABLE III. - VANGUARD III PENETRATION DATA

(FROM GODDARD RESEARCH CENTER)

Experimental parameters	
Number of segments (pressure capsules)	2
Exposed area per segment, sq ft	1.657
Thickness of exposed area, in.	0.027
Material exposed	Magnesium
Exposure data	
Exposure time (from launch), days	72
Number of segments surviving	2

TABLE IV. - THERMAL-VACUUM TEST RESULTS

[Individual sensor assemblies.]

Sensor number	Pressure, mm Hg	Duration, hr	Temperature, ^{o}F	Total time of cycles, hr	Comments
1	1×10^{-4}	20	230	--	Temperature control failed; sensor failed at 290° F
2	5×10^{-5}	66	190	--	Sensor failed when bleed valve was opened
3	5×10^{-5}	336	200	--	Removed for inspection
	6×10^{-4}	29	250	--	Heater failed
	2×10^{-5}	17	255	--	Increased temperature
	------	<1	300	--	Sensor failed at 300° F
4	5×10^{-6}	336	260	--	Removed for inspection
5	5×10^{-6}	336	260	--	Removed for inspection
	5×10^{-5}	341	-50 to 250	80	Removed for inspection
	5×10^{-5}	79	-40 to 200	23	Removed for inspection
6 and 7	5×10^{-5}	122	-30 to 190	23	Removed for inspection

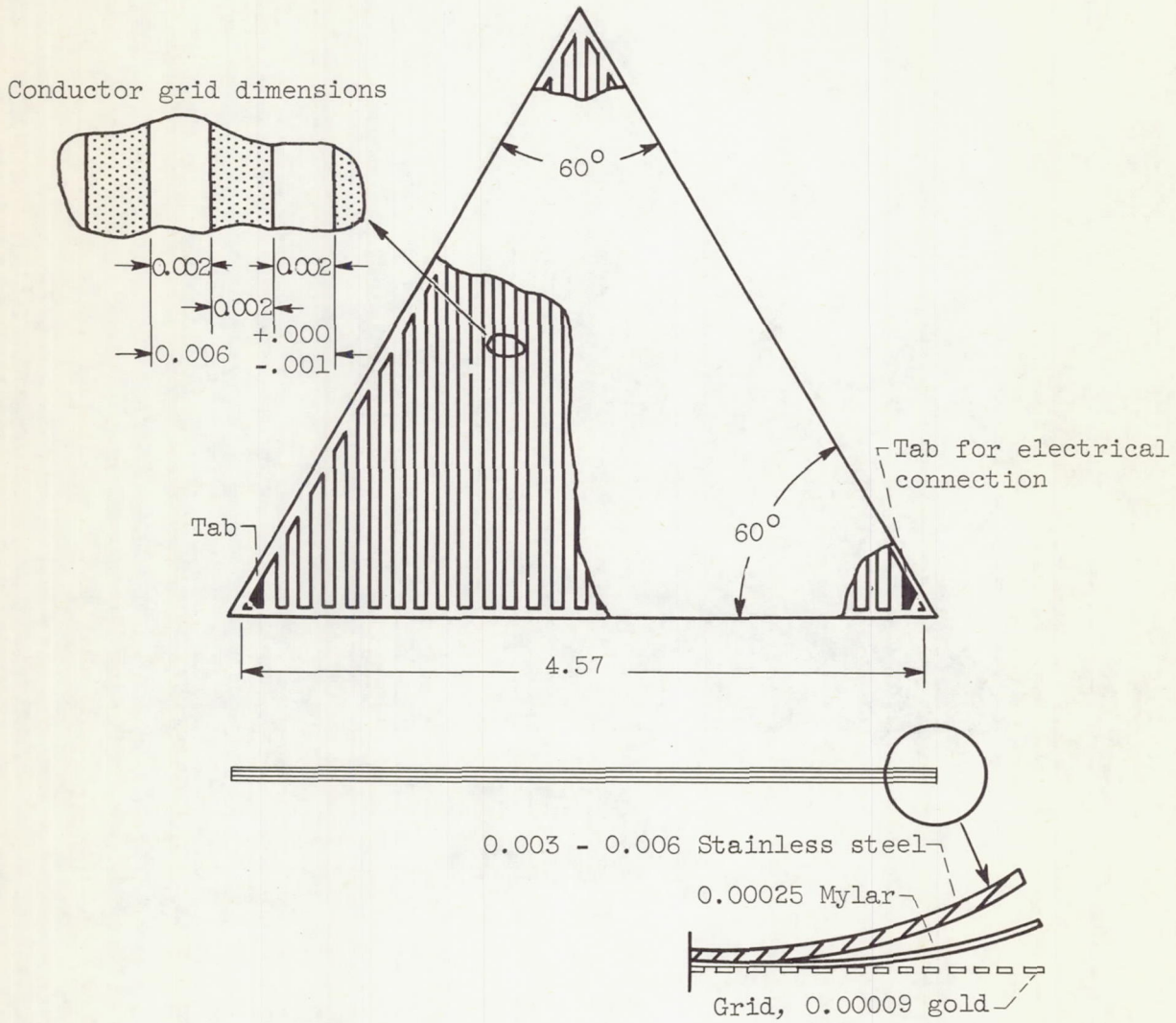

Figure 1. - Gold grid sensor. (All dimensions are in inches.)

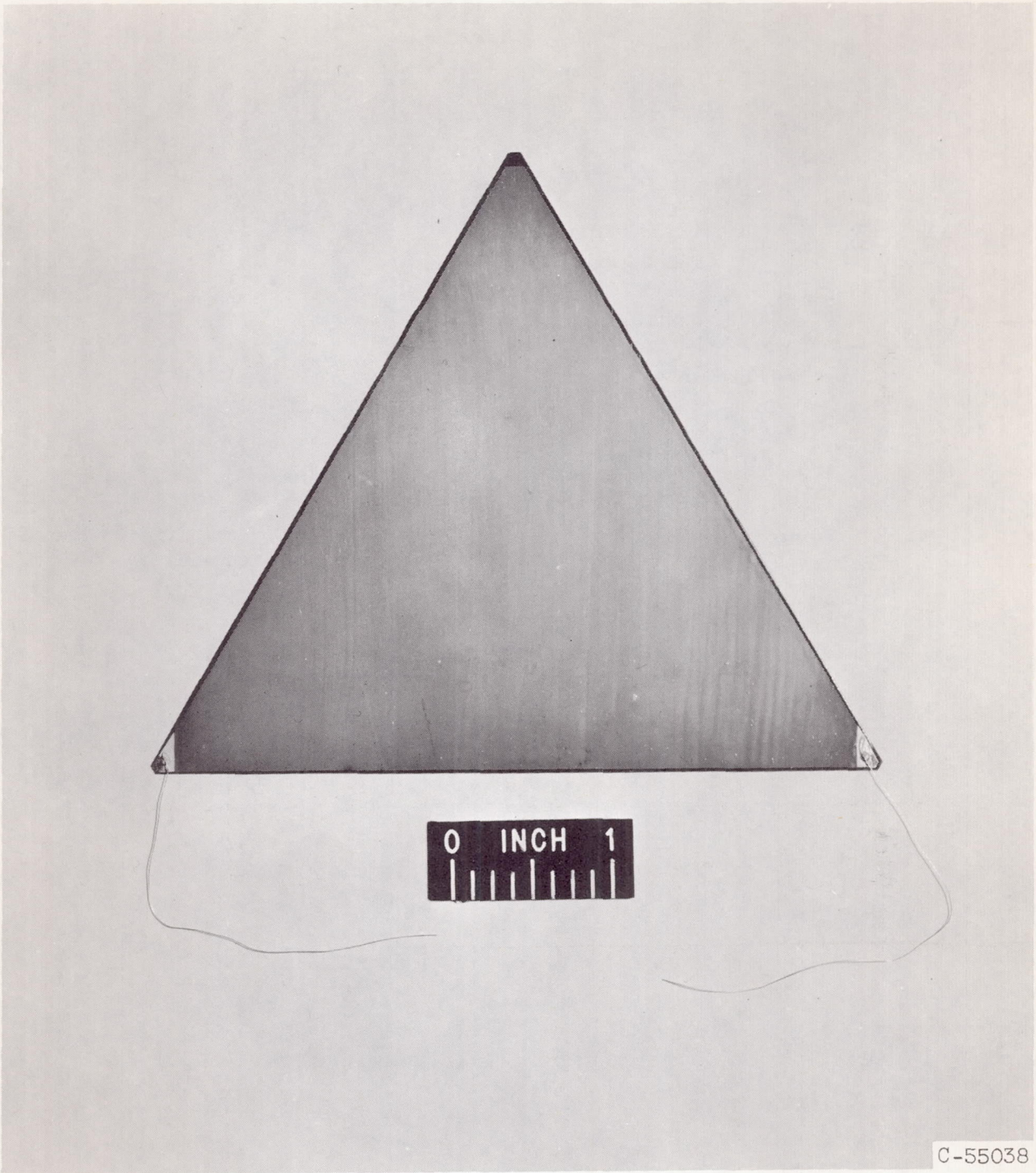

Figure 2. - Sensor with attached lead wires.

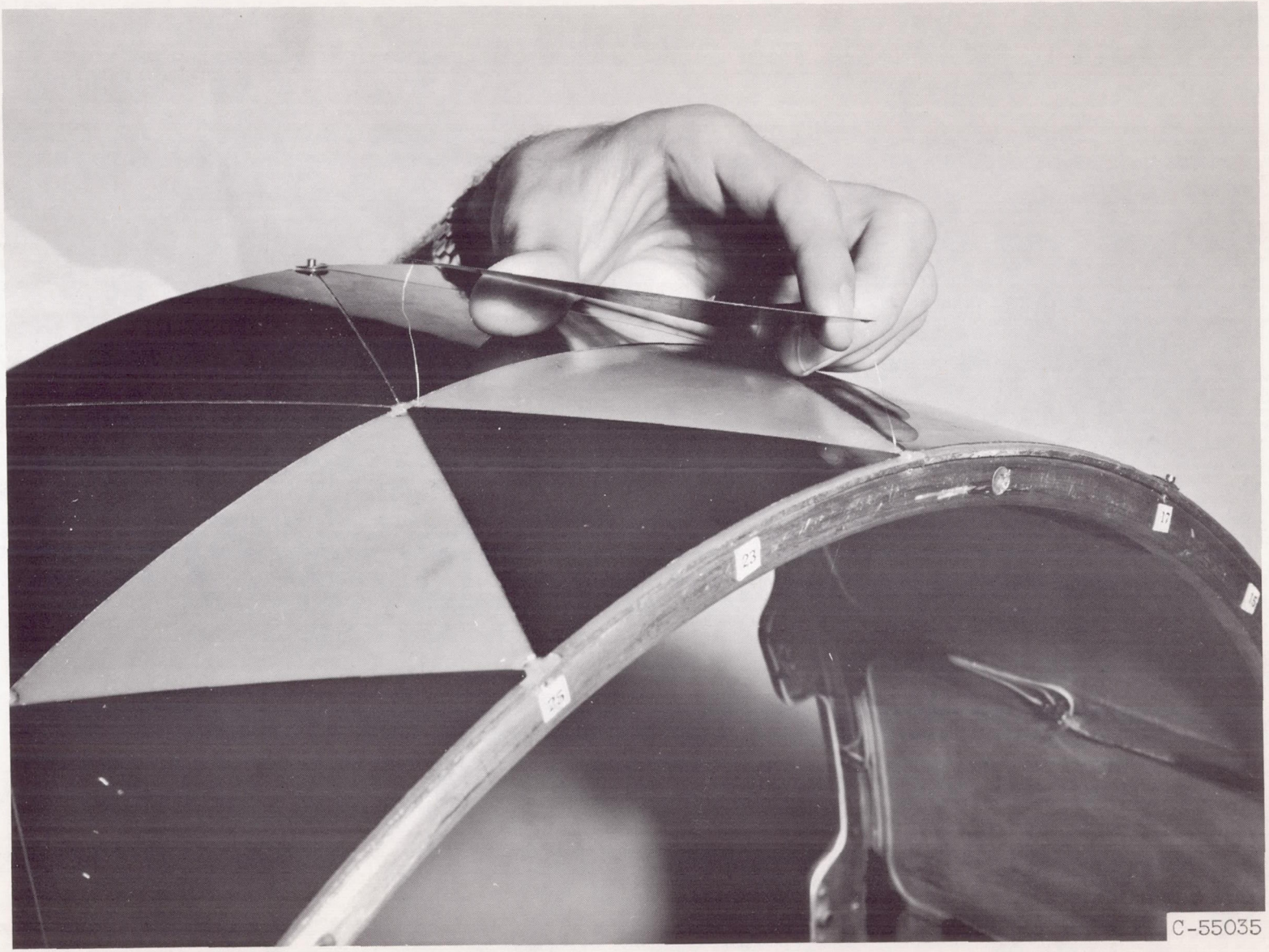

(a) Mounted sensors and satellite support structure.

Figure 3. - Sensor assembly details.

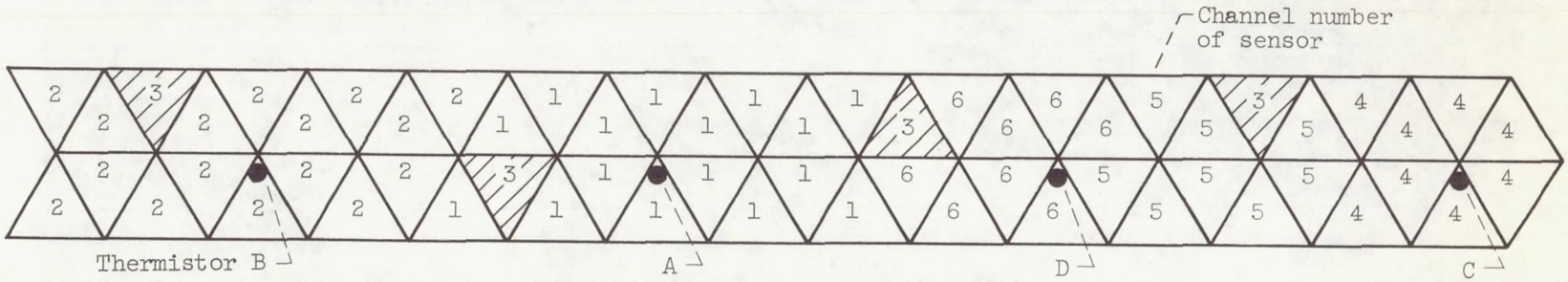

(b) Developed view showing sensor distribution by telemetry channel.

Figure 3. - Concluded. Sensor assembly details.

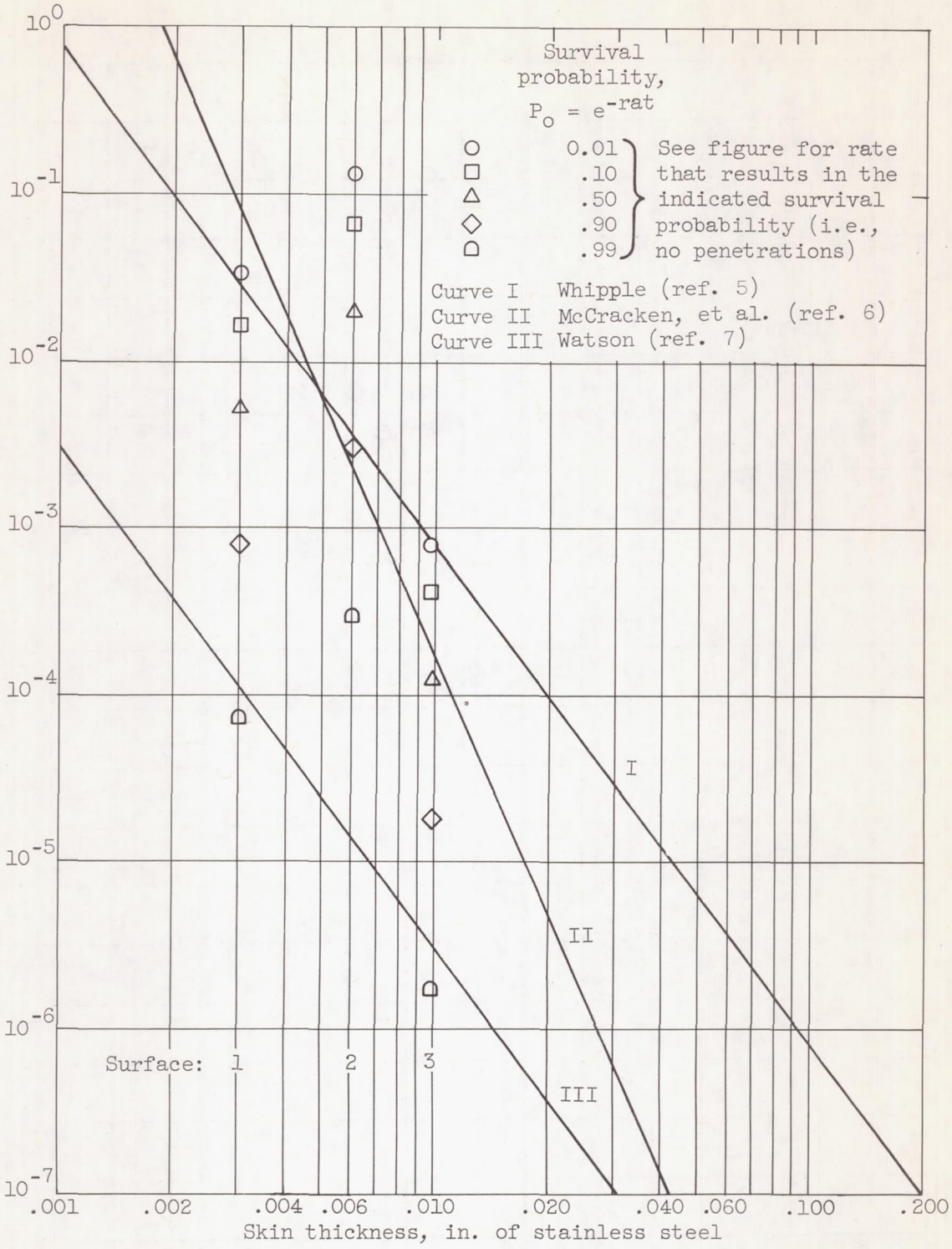

Figure 4. - Penetration rate estimates. Impact velocity, 15 kilometers per second; micrometeoroid density, 2.7 grams per cubic centimeter: Summers' penetration criteria for quasi-infinite targets (ref. 8) multiplied by 1.5.

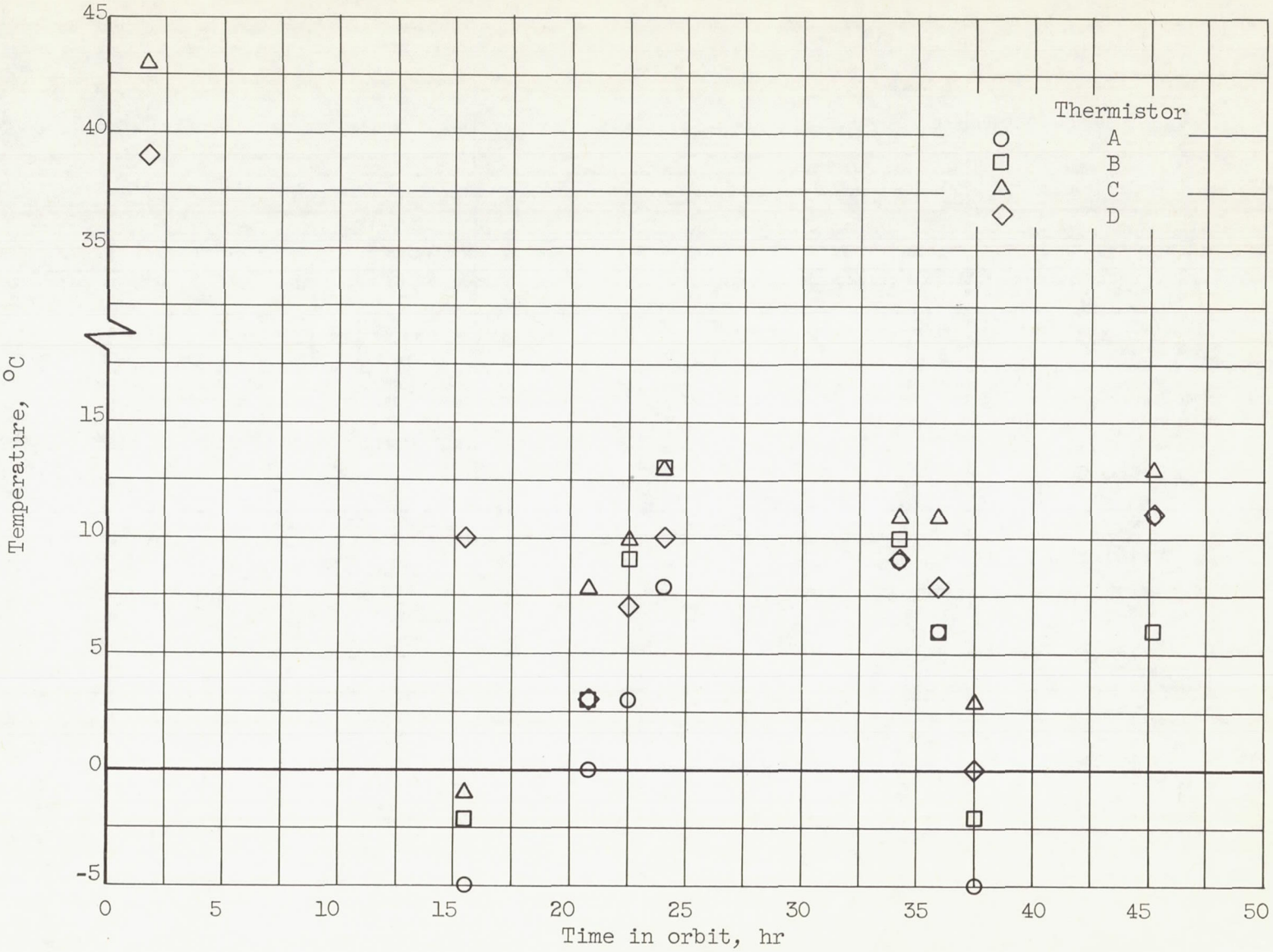

Figure 5. - Measured sensor temperatures.

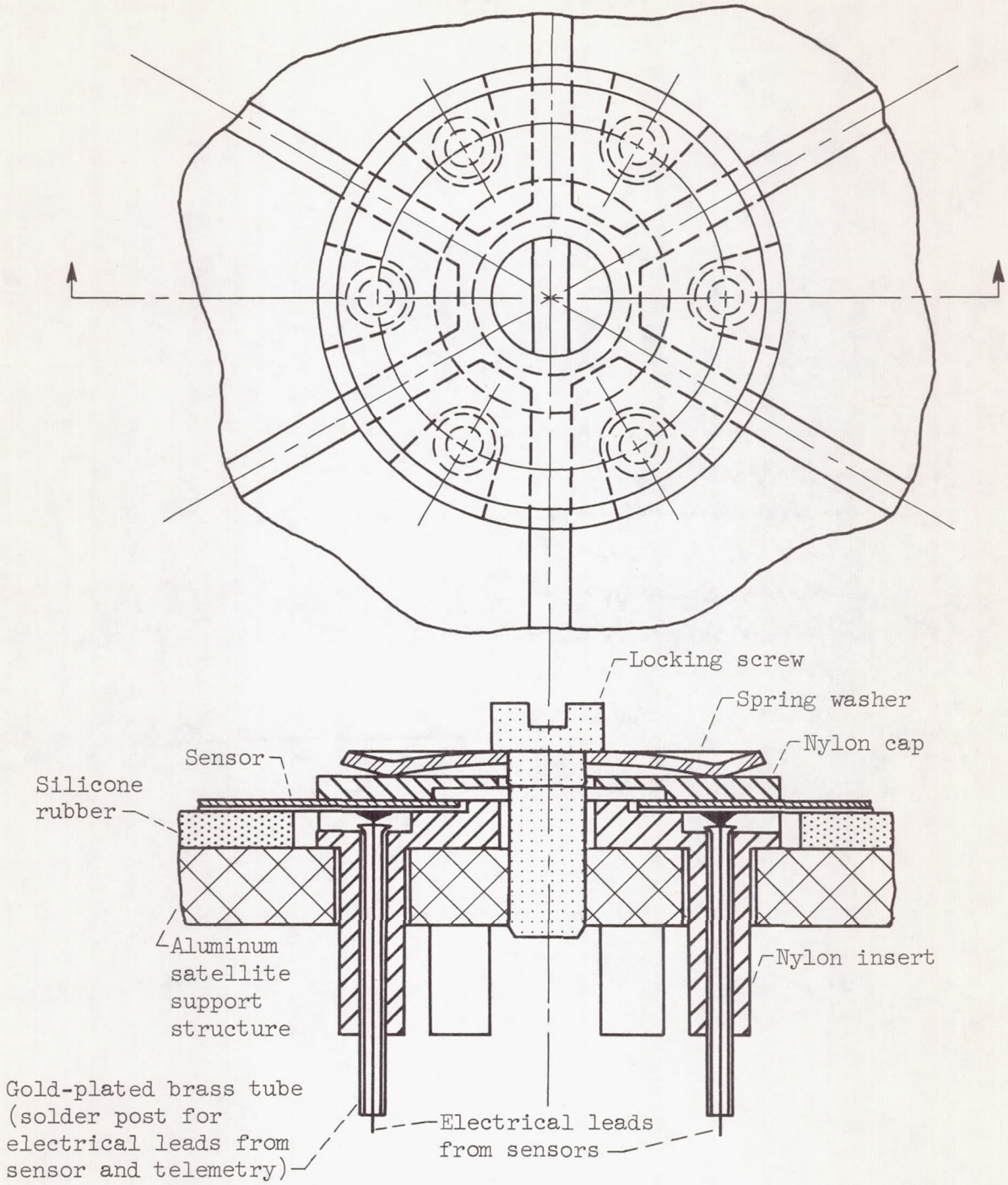

Figure 6. - Sensor electrical connections and mounting details.

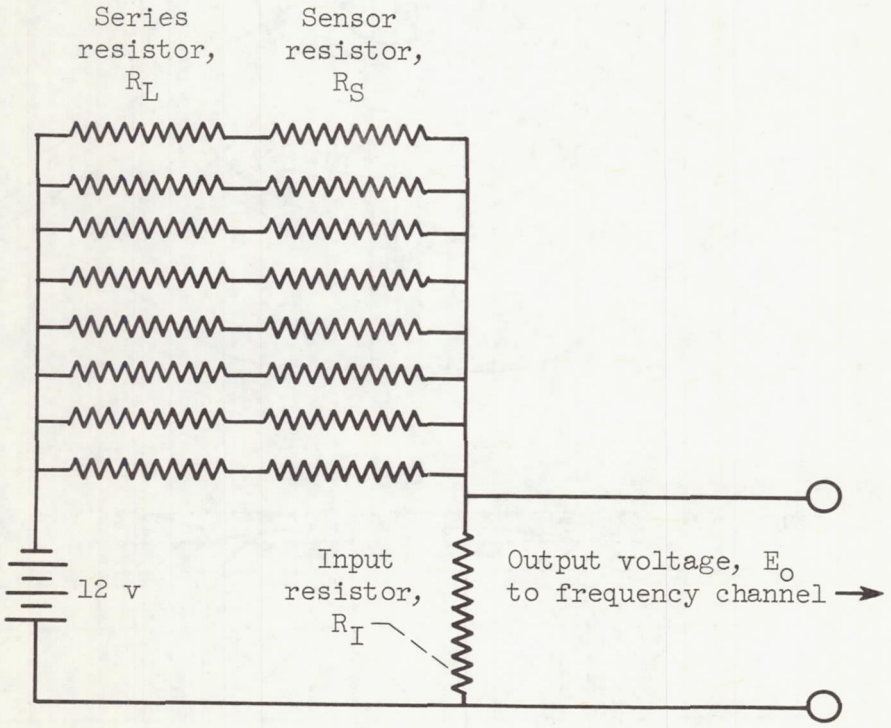

Figure 7. - Frequency channel circuit for sensor interrogation.

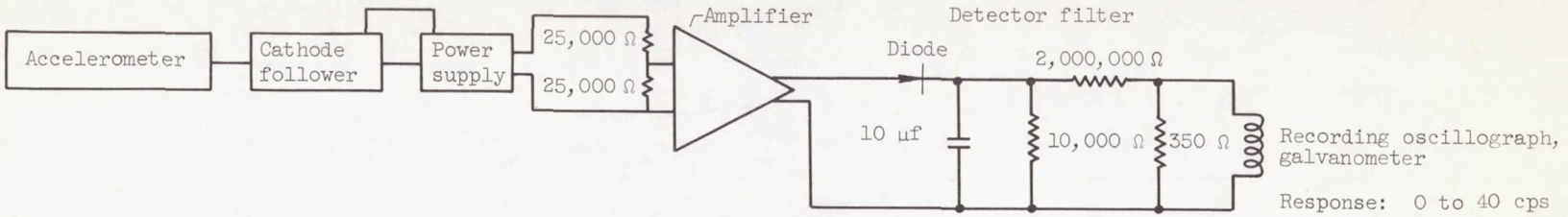

(a) Circuit for accelerometers 2 and 3.

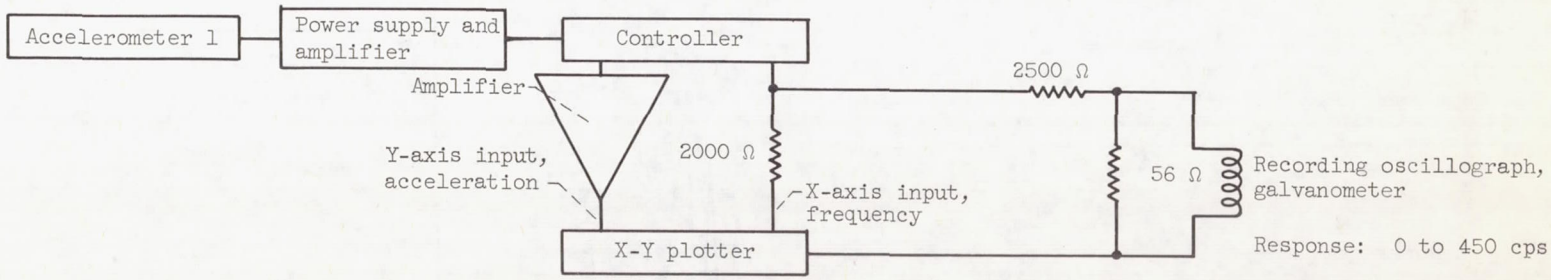

(b) Circuit for accelerometer 1.

Figure 8. - Acceleration measuring equipment for vibration testing.

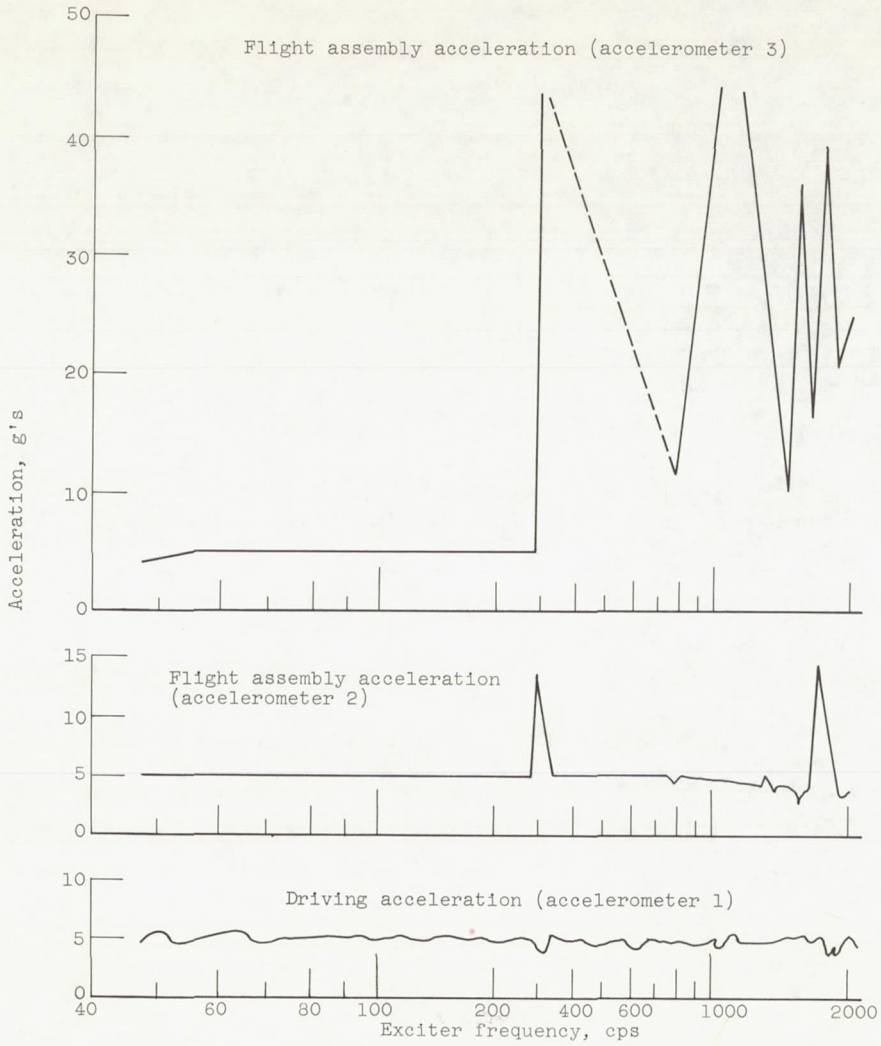

(a) Nominal 5-g driving acceleration. (Frequency sweep rate, 50 to 2000 cps at 2.8 octaves/min.)

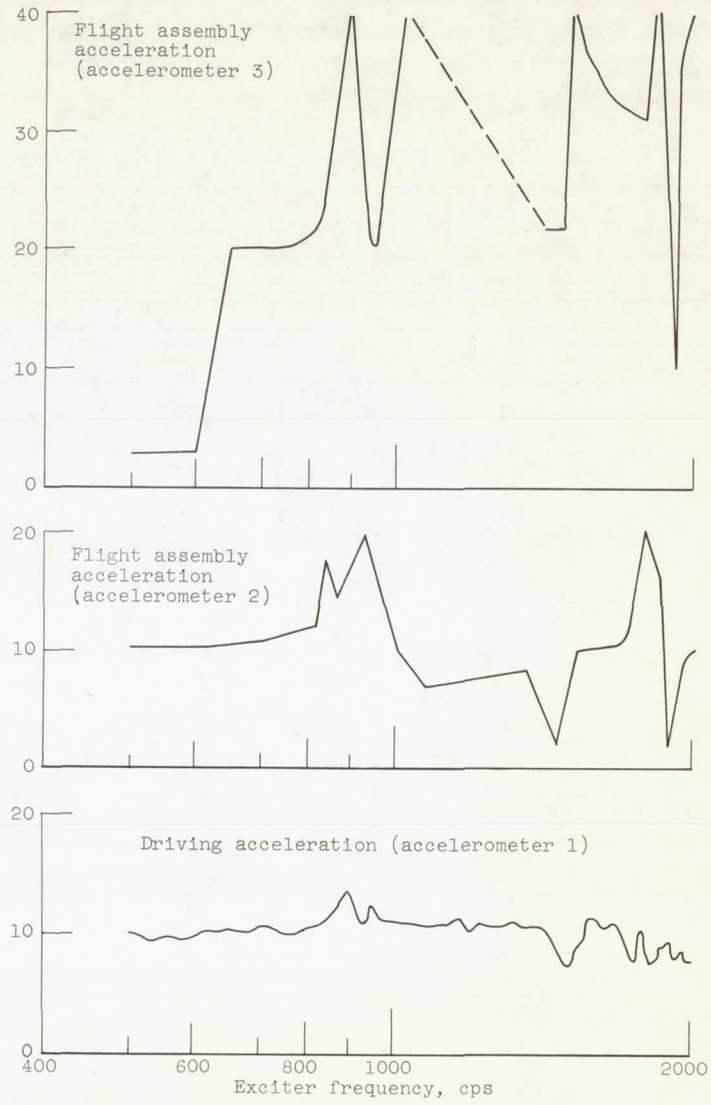

(b) Nominal 10-g driving acceleration. (Frequency sweep rate, 500 to 2000 cps at 2.8 octaves/min.)

Figure 9. - Vibration test results for second flight assembly.

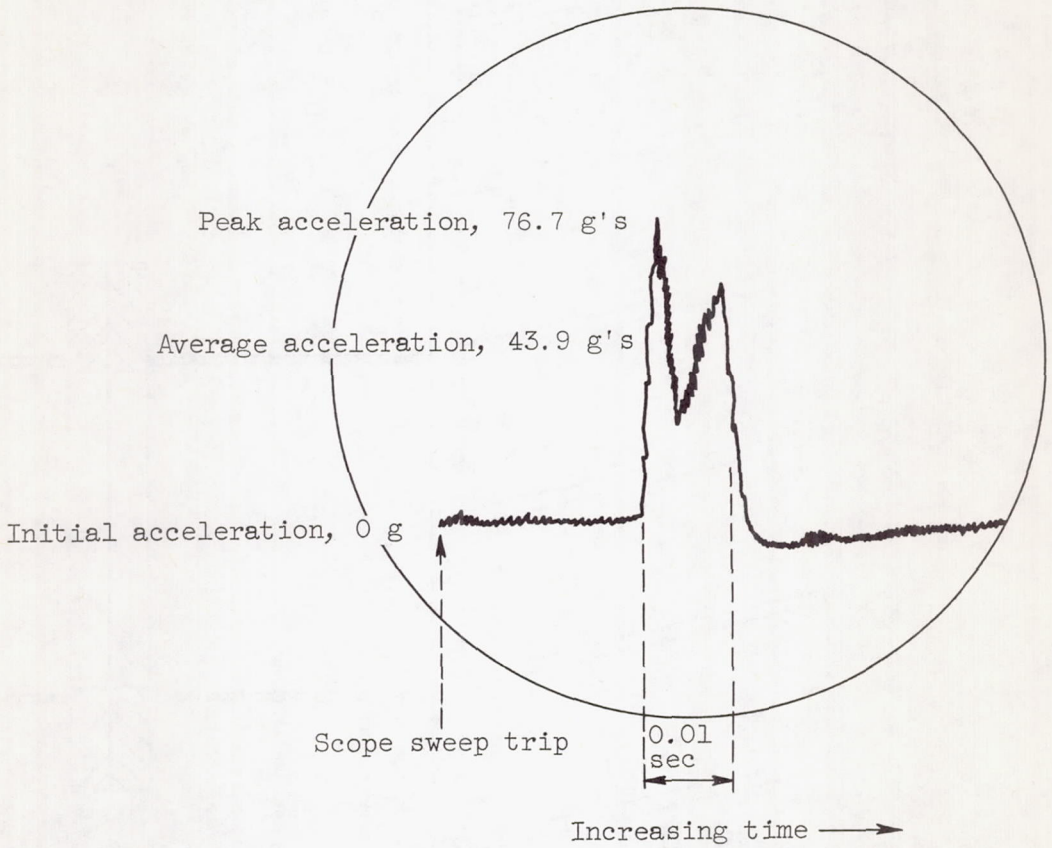

Figure 10. - Shock test results for second flight assembly (typical oscillograph camera record of drop test).

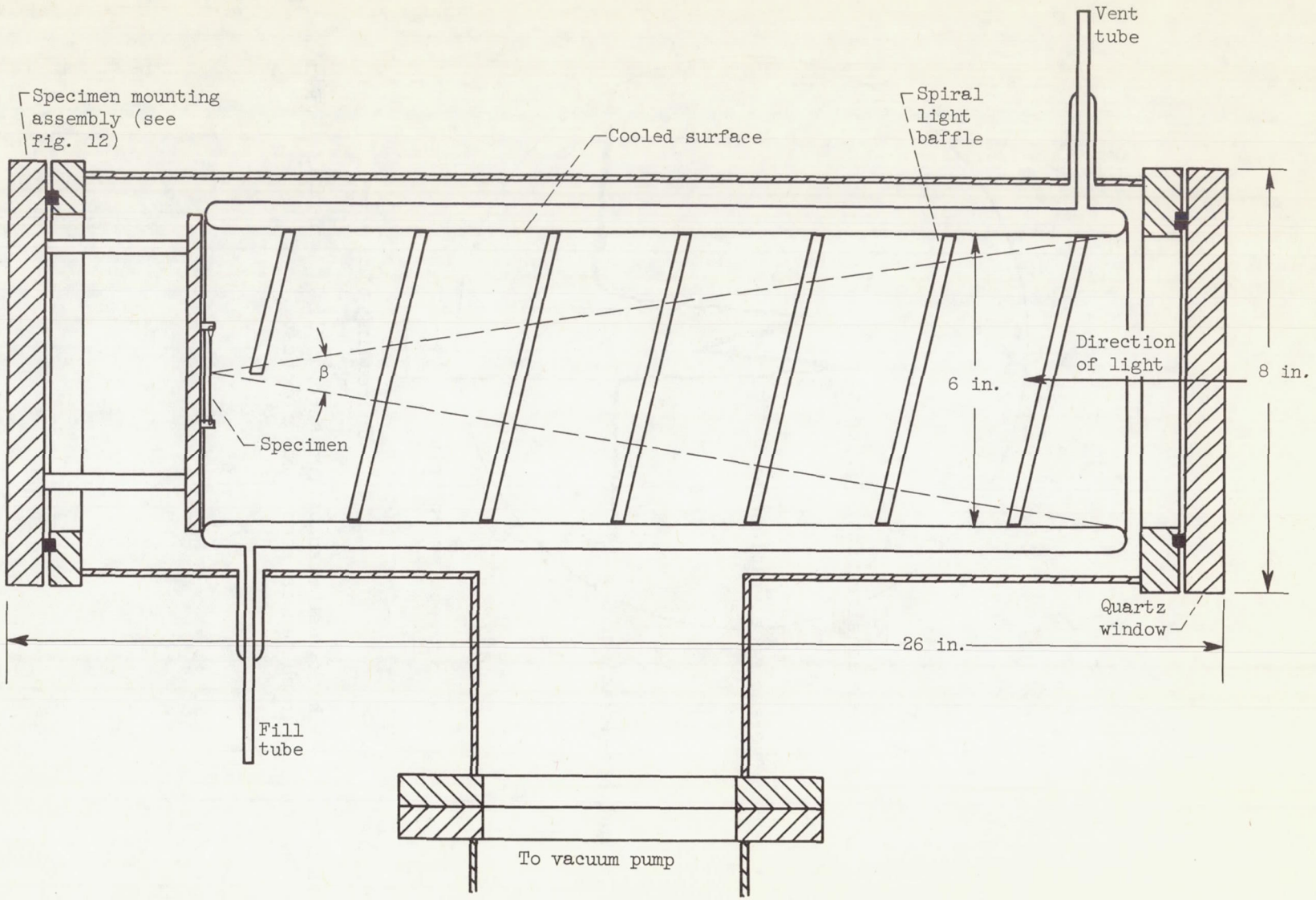

Figure 11. - Section view of thermal-vacuum chamber for equilibrium temperature measurement.

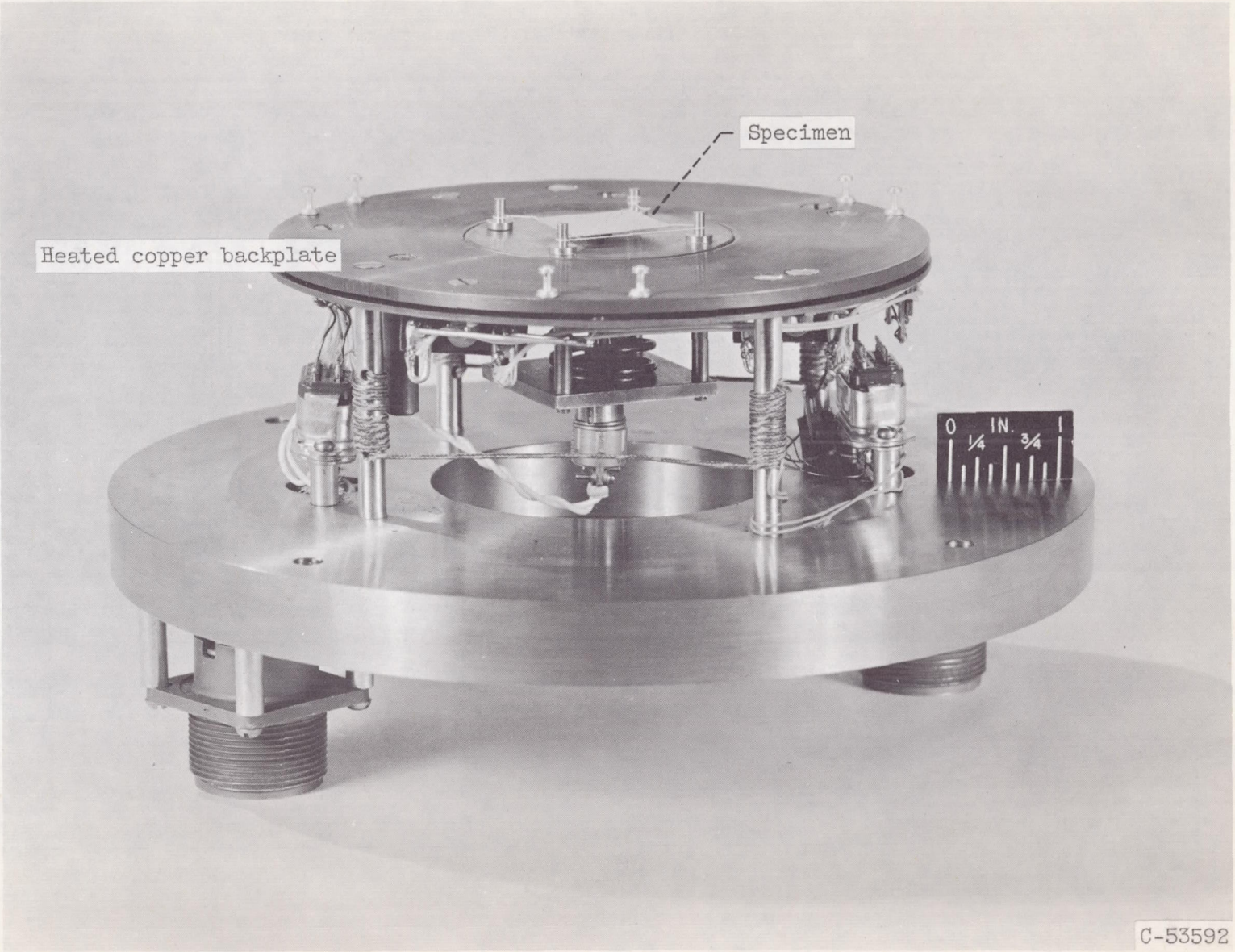

Figure 12. - Specimen mounting assembly of thermal-vacuum chamber.

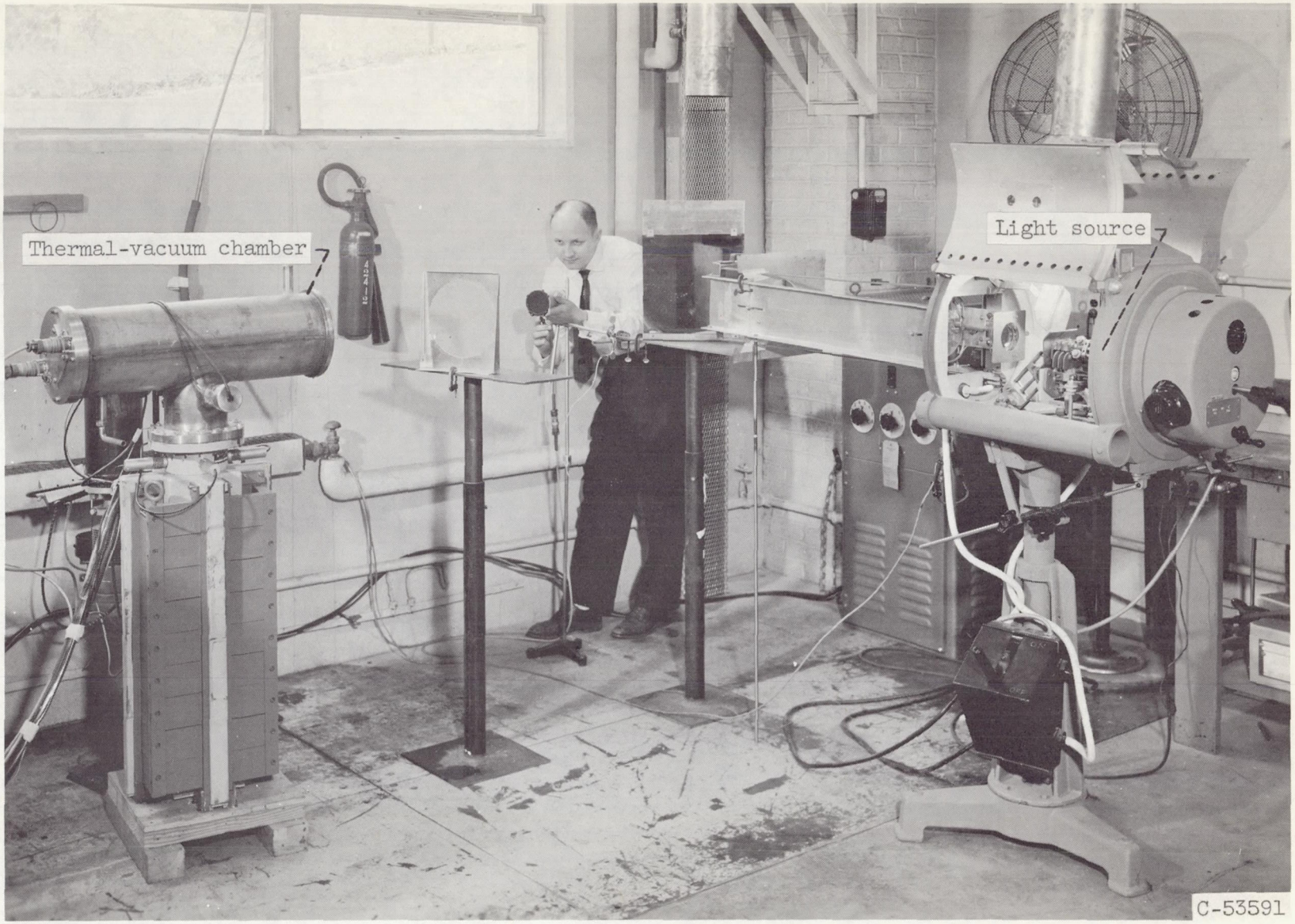

(a) Overall facility.

Figure 13. - Equilibrium temperature measurement equipment.

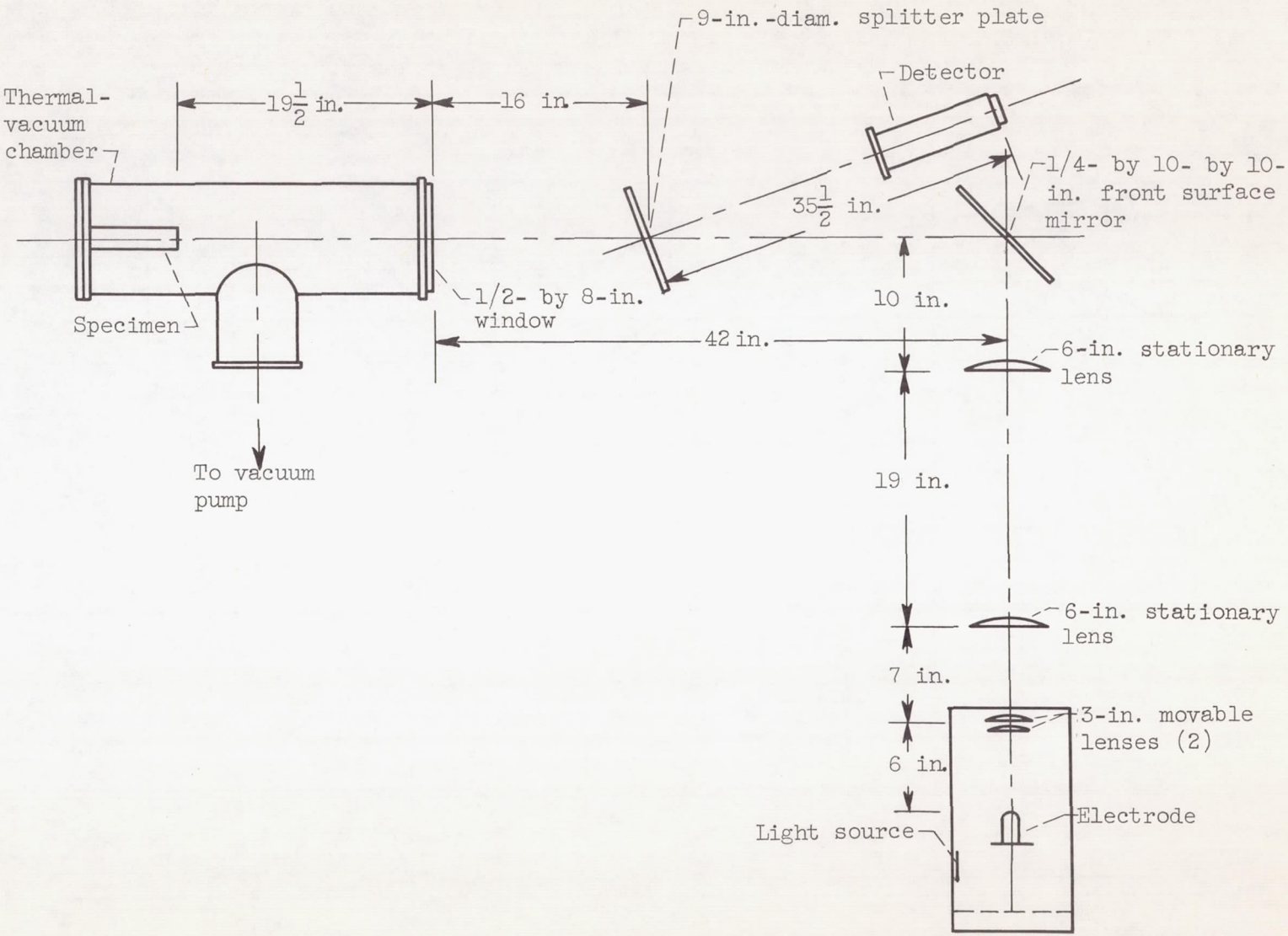

(b) Schematic diagram.

Figure 13. - Concluded. Equilibrium temperature measurement equipment.